Journal Pre-proof

Antidepressant response and stress resilience are promoted by CART peptides in GABAergic neurons of the anterior cingulate cortex

Yuki Funayama, Haiyan Li, Erina Ishimori, Ayako Kawatake-Kuno, Hiromichi Inaba, Hirotaka Yamagata, Tomoe Seki, Shin Nakagawa, Yoshifumi Watanabe, Toshiya Murai, Naoya Oishi, Shusaku Uchida

PII: S2667-1743(22)00002-7

DOI: https://doi.org/10.1016/j.bpsgos.2021.12.009

Reference: BPSGOS 98

To appear in: *Biological Psychiatry Global Open Science*

Received Date: 7 October 2021

Revised Date: 9 December 2021

Accepted Date: 27 December 2021

Please cite this article as: Funayama Y., Li H., Ishimori E., Kawatake-Kuno A., Inaba H., Yamagata H., Seki T., Nakagawa S., Watanabe Y., Murai T., Oishi N. & Uchida S., Antidepressant response and stress resilience are promoted by CART peptides in GABAergic neurons of the anterior cingulate cortex, *Biological Psychiatry Global Open Science* (2022), doi: https://doi.org/10.1016/j.bpsgos.2021.12.009.

Antidepressant response and stress resilience are promoted by CART peptides in GABAergic neurons of the anterior cingulate cortex

Authors:
Yuki Funayama[1,2], Haiyan Li[1], Erina Ishimori[1], Ayako Kawatake-Kuno[1], Hiromichi Inaba[1,2], Hirotaka Yamagata[3], Tomoe Seki[3], Shin Nakagawa[3], Yoshifumi Watanabe[3,4], Toshiya Murai[1,2], Naoya Oishi[1,*], and Shusaku Uchida[1,*]

Affiliations:
[1]SK Project, Medical Innovation Center, Kyoto University Graduate School of Medicine, 53 Shogoin-Kawahara-cho, Sakyo-ku, Kyoto 606-8507, Japan
[2]Department of Psychiatry, Kyoto University Graduate School of Medicine, 54 Shogoin-Kawahara-cho, Sakyo-ku, Kyoto 606-8507, Japan
[3]Division of Neuropsychiatry, Department of Neuroscience, Yamaguchi University Graduate School of Medicine, 1-1-1 Minami-Kogushi, Ube, Yamaguchi 755-8505, Japan
[4]Present address: Southern TOHOKU Research Institute for Neuroscience, Southern TOHOKU General Hospital, 7-115 Yatsuyamada, Koriyama, Fukushima 963-8052, Japan

*Correspondences:
Shusaku Uchida, Ph.D. (e-mail: uchida.shusaku.3n@kyoto-u.ac.jp),
Naoya Oishi, M.D., Ph.D. (e-mail: noishi@kuhp.kyoto-u.ac.jp)

Running title:

CART peptides mediate antidepressant response

Keywords:

Antidepressant response; Stress resilience; Depression; Transcriptome; Anterior cingulate cortex; GABAergic neurons

Abstract

Background:

A key challenge in the understanding and treatment of depression is identifying cell types and molecular mechanisms that mediate behavioral responses to antidepressant drugs. As treatment responses in clinical depression are heterogeneous, it is crucial to examine treatment responders and nonresponders in preclinical studies.

Methods:

We utilized the large variance in behavioral responses to chronic treatment with multiple class of antidepressant drugs in different inbred mouse strains and classified the mice into responders and nonresponders based on their response in the forced swim test. Medial prefrontal cortex tissues were subjected to RNA sequencing to identify molecules that are consistently associated across antidepressant responders. We developed and employed virus-mediated gene transfer to induce the gene of interest in specific cell types and performed forced swim test, sucrose preference, social interaction, and open field tests to investigate antidepressant-like and anxiety behaviors.

Results:

Cocaine- and amphetamine-regulated transcript peptide (*Cartpt*) expression was consistently upregulated in responders to four types of antidepressants but not in nonresponders in different mice strains. Responder mice given a single dose of ketamine, a fast-acting non-monoamine-based antidepressant, exhibited high CART peptide expression. CART peptide overexpression in the GABAergic neurons of the anterior cingulate cortex (aCC) led to antidepressant-like behavior and drove chronic stress resiliency independently of mouse genetic background.

Conclusions:

These data demonstrate that activation of CART peptide signaling in GABAergic neurons of the aCC is a common molecular mechanism across antidepressant responders and that this pathway also drives stress resilience.

Introduction

Typical antidepressants such as tricyclic antidepressants and selective serotonin and/or noradrenaline reuptake inhibitors (SSRIs/SNRIs), which are used for treating major depressive disorder (MDD), target monoamine systems that have widespread effects throughout the central nervous system. However, approximately 60% of patients do not respond to a single trial, and 30%–40% of patients do not remit from depression even after multiple treatment attempts (1). Treatment responses in clinical depression vary, and the treatment efficacy becomes evident after weeks or months, which necessitated the development of more effective treatments.

The prefrontal cortex (PFC) has emerged as a key brain region in MDD pathophysiology and in depression treatment (2-4). Neuroimaging studies of MDD have reported altered activity in the PFC (3, 5-7). Clinical evidence suggests the involvement of PFC GABA-related molecules in MDD pathophysiology and antidepressant actions (8-11). Preclinical studies indicated that the medial PFC (mPFC), which includes the prelimbic, infralimbic, and anterior cingulate cortices, is associated with both depression-like behaviors as well as with induction of antidepressant-like response in rodents (12-15). Thus, mPFC may exert strong regulation over mood-related behaviors.

A key challenge in understanding and ultimately treating depression is identifying molecular mechanisms that mediate behavioral responses to antidepressants (16). As mentioned above, given that antidepressant responses vary widely among humans, it is important to stratify animals into subgroups of responders and those of non-responders to antidepressant treatments, to better understand the mechanism of action of antidepressant drugs. In addition, the genetic backgrounds of mice influence their sensitivity to antidepressants (17-19), whereas the common molecular mechanisms driving antidepressant-like behaviors across inbred mice strains remain unknown. Furthermore, it remains unclear whether there are common transcriptional signatures across multiple types of antidepressant drugs. Therefore, identifying molecules that are consistently regulated in multiple classes of antidepressant responders and are

commonly regulated in various inbred mouse strains may provide insight on the molecular mechanisms targeted by both established and experimental pharmacotherapies.

Herein, we developed an animal-based approach modeling the heterogeneity in the response to chronic treatment with four classes of antidepressants in three mouse strains. Our data revealed fundamental differences in molecular signatures between responders and nonresponders and implicated specific molecules in the development of anti-depression drugs.

Materials and Methods

Additional information is available in the *Supplement*.

Animals

All procedures were performed according to the Guide for Animal Care and Use of Yamaguchi University and Kyoto University and were approved by the Institutional Animal Care and Use Committees of Kyoto University and Yamaguchi University.

Antidepressant treatment

For continuous treatment with imipramine hydrochloride (IMI), maprotiline hydrochloride (MPR), sertraline hydrochloride (SRT), and duloxetine hydrochloride (DLX), the drugs were dissolved in tap water to a concentration of 160 mg/L (17, 20, 21) and administered for 3 weeks (chronic) or 5 days (subchronic). Vehicle-treated animals received drinking water regularly.

Social defeat stress (SDS)

Chronic SDS (CSDS) and subchronic and mild SDS (smSDS) were administered as reported previously (22-24).

Behavioral tests

All behavioral experiments were performed between 9:00 and 15:00 in a blinded fashion as reported previously (21, 23, 25).

Forced swim test (FST). Mice were placed in a cylinder of water, they were allowed to swim around freely for 6 min, and their immobility time was measured.

Sucrose preference test (SPT). After a 16-h liquid deprivation, mice were

given two bottles, one with 1.5% sucrose and another with tap water for 4 h. The sucrose preference was calculated as the percentage of sucrose solution consumed relative to the total intake.

Open field test (OFT). Mice were individually placed in the center of an open field box and allowed to explore the arena freely for 5 min. The percentage of time spent in the center area was measured automatically using an ANY-maze video-tracking system.

Social interaction test (SIT). Mice were placed in a test chamber with an empty wire-mesh cage as a first term for 3 min, then with an unfamiliar CD1 mouse enclosed in the wire-mesh cage as a second term for 3 min. The time spent in the area surrounding the wire-mesh cage was measured in both sessions automatically using an ANY-maze tracking system.

RNA analysis

Total RNA from mPFC regions, including the prelimbic, infralimbic, and anterior cingulate cortices (bregma 1.98–0.98 mm) was extracted using the Direct-zol RNA Microprep according to the manufacturer's instructions. An Illumina HiSeq system was used for RNA-seq. Raw data were deposited in GEO (GSE168172). The sequences of all primers used in quantitative PCR (Q-PCR) are listed in Supplementary Table S1. RNAscope from brain sections (anterior part of Cg1/Cg2, bregma 1.70–1.18 mm) was performed as described previously (23).

Statistical analysis

Complete statistical summaries are provided in Supplementary Table S2. GraphPad Prism 7.0 and SPSS Statistics 25 were used to perform Student's *t*-tests, unpaired *t*-test, Wilcoxon test, Kruskal–Wallis test, and one- or two-way analysis of variance (ANOVA) as appropriate to determine statistical differences. For ANOVA, significant effects were followed by Tukey's *post-hoc* comparison. For multiple comparisons, Dunnett's test were used and adjusted *P*-values were adopted. To assess data normality, Kolmogorov–Smirnov and/or Shapiro–Wilk tests were used. In all cases, comparisons were considered significant at $P < 0.05$. All data are presented as means ± SEM.

Results

Modeling heterogeneity in antidepressant treatment response

We aimed to identify molecule(s) promoting behavioral responses to antidepressants regardless of the genetic background and antidepressant class. Therefore, we characterized antidepressant-like behaviors in BALB/c (BALB), C57BL/6J (B6), and DBA/2 (DBA) inbred mice after chronic treatment with IMI, MPR, SRT, and DLX, as a tricyclic antidepressant, tetracyclic antidepressant, SSRI, and SNRI, respectively. We performed the FST, which is commonly used to assess the efficacy of antidepressant response in rodents (26-29), and measured the immobility time on the day before treatment (FST-1) (Fig. 1A). Mice were then treated with antidepressants or vehicle via drinking water for 21 days and subsequently subjected to a second forced swim test (FST-2). The antidepressant response was determined as the percentage change in immobility time from baseline (FST-1). We found a strain difference in antidepressant response (Fig. 1B-D). In BALB mice, IMI and SRT had a significant effect on percentage change in immobility time (Fig. 1B), whereas in B6 and DBA mice, MPR and DLX had significant effects (Fig. 1C and D).

As there was a large individual difference in antidepressant response (Fig. 1B-D), we estimated the response ratio by dividing the immobility time of FST-1 by that of FST-2 and identified a treatment responder or nonresponder mouse with a cutoff value using a traditional mean ± 2SD method. Mice with response ratios larger than the cutoff values (i.e., mean + 2SD) in each strain were defined as responders (Fig. 1E-G). The distribution pattern of the response to antidepressants significantly differed among strains, with overall 22.5%–45% of the mice being responders to chronic antidepressant treatment (Fig. 1H). In previous studies, nearly 30% of patients with MDD achieved remission after their first course of typical antidepressant pharmacotherapy (1, 30), suggesting that our models could help provide translational and mechanistic insights into the mechanism of behavioral responses to antidepressants.

Differential expression signatures of antidepressant responders and nonresponders

We performed RNA-seq to compare genome-wide transcriptional changes in the responders and nonresponders. We selected the BALB strain, as previous reports showed that this strain could be a stress-vulnerable model (21, 23, 31). In addition, we selected SRT and DLX for RNA-seq due to their increasing prescription worldwide (32, 33). mPFC tissue punches from five BALB mouse groups were subjected to RNA-seq: SRT-responders (SRT-R), SRT-nonresponders (SRT-NR), DLX-responders (DLX-R), DLX-nonresponders (DLX-NR), and vehicle-treated mice. Differentially expressed genes (DEGs) were profiled in these conditions (Fig. 2A, Tables S3-S7). We identified few common DEGs that were consistently upregulated in the SRT-R, SRT-NR, DLX-R, and DLX-NR groups relative to the vehicle. RNA-seq revealed that seven genes (*Nab2*, *Egr1*, *Egr2*, *Per1*, *c-fos*, *Otud1*, and *Dusp6*) were upregulated in both responders and nonresponders treated with SRT and DLX (Fig. 2B and Table S3a). This result was validated using Q-PCR (Fig. 2C–I). We next identified DEGs that were upregulated/downregulated in either SRT-R, SRT-NR, DLX-R, or DLX-NR relative to the vehicle (Fig. 2J–M and Table S3b). The Gene Ontology (GO) profile analysis results at the biological process level of DEGs in each subgroup are shown in Figure 2N. Finally, we identified DEGs that were uniquely regulated in responders and nonresponders treated with SRT or DLX (Fig. S1 and Table S4).

Identification of consistently regulated genes

Sixty-five DEGs were commonly regulated by SRT and DLX in responders (upregulated/downregulated in both SRT-R and DLX-R but not in SRT-NR or DLX-NR, relative to the vehicle) (Fig. 3A,B, Table S5a). Fifty-three DEGs were commonly regulated by SRT and DLX in nonresponders (upregulated/downregulated in both SRT-NR and DLX-NR but not in SRT-R or DLX-R, relative to the vehicle) (Fig. S2, Table S5b). GO enrichment analysis revealed that genes that were consistently regulated in SRT and DLX responders were significantly enriched for the neuropeptide signaling pathway (Fig. 3C,E), and network graphs showed that the gene encoding cocaine- and

amphetamine-regulated transcript (*Cartpt*) was commonly implicated in SRT and DLX responders (Fig. 3D and 3F). We then validated the mRNA expression of *Cartpt*, *Npas4*, *Col1a2*, *Col4a3*, *Creb3l4*, *Cxcl16*, *Epn3*, and *Rsph6a*, which were DEGs consistently upregulated by SRT and DLX in responders in the RNA-seq analysis and were protein coding, mPFC-expressed genes (Allen Brain Atlas: http://mouse.brain-map.org/). Q-PCR results revealed the significantly altered expression of *Cartpt*, *Npas4*, *Col1a2*, *Epn3*, and *Rsph6a* in antidepressant-responder BALB, B6, or DBA mice (Figs 3G-I and S3); among them, *Cartpt* expression was consistently and significantly upregulated in all antidepressant responders but not in nonresponders (Fig. 3G-I). These findings suggest that neuropeptide signaling via CART peptides is associated with antidepressant response.

We also examined the effect of subchronic antidepressant treatment on *Cartpt* mRNA expression in the aCC of B6 mice. After subchronic DLX treatment, FST-2 was performed (Fig. S4A). There was no significant difference in immobility time between vehicle- and DLX-treated mice (Fig. S4B), and only 5 out of 44 mice (11.4%) treated with DLX were responders (Fig. S4C). Importantly, DLX-responder mice exhibited a significantly higher *Cartpt* mRNA expression relative to vehicle-treated mice (Fig. S4D), suggesting that *Cartpt* induction promotes a behavioral response to antidepressants.

Ketamine, a fast-acting non-monoamine-based antidepressant, has emerged as a novel therapeutic agent. We tested whether ketamine upregulated *Cartpt* mRNA expression in the aCC of B6 mice. Consistent with a previous report (26), the FST immobility time was significantly decreased 24 h after ketamine treatment (Fig. S5A-C). *Cartpt* mRNA expression was significantly higher in ketamine treatment responders (48 h after the ketamine injection) than that in the saline control (Fig. S5D). Collectively, these data suggest that CART peptide promotes the behavioral effects of traditional antidepressants and is associated with the antidepressant-like effects of ketamine.

CART peptide induction in GABAergic neurons of the aCC of antidepressant responders

To identify specific cell types in which *Cartpt* expression is altered in antidepressant responders, we used the translating ribosome affinity purification (TRAP) technique, which enables identification of all proteins synthesized in a target cell population and alterations of this translational profile in response to pharmacological perturbations (34, 35). vGat-Cre and vGlut-Cre mice were bred with transgenic mice expressing EGFP-tagged ribosomal protein L10a (EGFP-L10a) to establish vGat-TRAP and vGlut-TRAP mice. These mice expressed EGFP-L10a in GABAergic and glutamatergic neurons, respectively, enabling the identification of the cell type in which *Cartpt* expression is altered in responders (Fig. 3J). vGat-TRAP and vGlut-TRAP mice were administered IMI, MPR, SRT, or DLX for 3 weeks and then divided into two groups (responders and nonresponders) based on their response ratio in the FST (Fig. 1). Subsequently, EGFP-labeled polysomes from mouse mPFC tissue punches were affinity-purified to enrich cell-specific, polysome-bound, translating mRNAs. Q-PCR revealed that vGat-TRAP mice had significantly elevated *Cartpt* expression in GFP-immunoprecipitated samples in antidepressant responders, but not in nonresponders, when compared to vehicle-treated mice (Fig. 3K). vGlut-TRAP mice did not show a significantly elevated *Cartpt* expression in GFP-immunoprecipitated samples in antidepressant responders (Fig. 3L). These results suggest that *Cartpt* expression is induced in GABAergic neurons in antidepressant responders. For confirmation, we assessed *Cartpt* mRNA expression histologically using RNAscope. *Cartpt* mRNA was enriched in the aCC but was low or undetectable in the prelimbic and infralimbic areas (data not shown); moreover, in the aCC, the majority of *Cartpt*-expressing cells were *Slc32a1*-positive GABAergic neurons, with few *Cartpt*-expressing cells overlapping with *Camk2a*-positive glutamatergic neurons (Fig. 3M). These results suggest that CART peptide signaling in GABAergic neurons of the aCC is associated with antidepressant response.

Effects of CART peptide overexpression in antidepressant-like behavior and behavioral response to chronic stress

To assess whether CART peptide induction in GABAergic neurons of the aCC is sufficient to induce an antidepressant-like behavior, we injected a Cre-dependent adeno-associated virus (AAV) expressing Cartpt (AAV-Cartpt) or control tdTomato (AAV-tdTomato) into the bilateral aCC of vGat-Cre or vGlut-Cre mice (C57BL/6J background) (Fig. 4A). These mice were tested using FST under non-stress conditions and subjected to chronic CSDS for 10 days; their behaviors were tested via the SIT, SPT, and OFT (Fig. 4B). Histological analysis confirmed successful transgene expression in the aCC of vGat-Cre and vGlut-Cre mice (Fig. 4C). Behaviorally, CART peptide overexpression in GABAergic neurons led to significantly decreased FST immobility time (Fig. 4D). Mice expressing control tdTomato showed significantly a decreased social interaction (SI) ratio in SIT, decreased sucrose preference in SPT, and lower percent time spent in the center in OFT after CSDS exposure when compared to nonstressed controls. In contrast, mice overexpressing CART peptide did not exhibit significant effects of CSDS (Fig. 4E-G). Mice overexpressing CART peptide in glutamatergic neurons showed comparable behaviors to those of mice expressing control tdTomato in FST, and CART peptide overexpression did not affect any behavior in SIT, SPT, and OFT as animal models of depression (Fig. 4H-K). These results suggest that CART peptide induction in GABAergic neurons of the aCC is sufficient for inducing an antidepressant-like behavior and chronic stress resiliency.

Behavioral effects of CART peptide induction in GABAergic neurons of the aCC in BALB mice

We investigated whether the antidepressant response afforded by CART peptide is independent of mouse genetic background. First, we developed a novel inhibitory neuron-specific promoter, with a length of 1.3 kb of the *Gad1* gene promoter and validated the specificity of this AAV. We injected AAVs

expressing mCherry under the control of *Gad1* promoter (AAV-Gad1-mCherry) into the aCC of vGlut-Cre::GFP-L10a and vGat-Cre::GFP-L10a mice (Fig. 5A). Histological analyses revealed that the majority of mCherry-positive cells co-localized with GFP-positive GABAergic neurons (77.8%) in vGat-Cre::GFP-L10a mice, whereas few mCherry-positive cells co-localized with GFP-positive glutamatergic neurons (5.1%) in vGat-Cre::GFP-L10a mice (Fig. 5B and C).

Therefore, we injected either AAV-Gad1-Cartpt or AAV-Gad1-mCherry into the bilateral aCC region of BALB mice (Fig. 5D). Three weeks after the surgery, the mice were subjected to FST and SIT (SIT-1) in non-stress conditions, followed by re-evaluation of their behaviors in SIT (SIT-2) following stress exposure (Fig. 5E). Because BALB is vulnerable to stress (21, 23), we subjected the mice to a 5-day smSDS regimen, which is an abbreviated and subthreshold version of CSDS that is sufficient for inducing a depression-like phenotype in the BALB strain (23). We found significantly decreased FST immobility time (Fig. 5F) but comparable social interaction time in SIT-1 (Fig. 5G) in mice injected with AAV-Gad1-Cartpt relative to AAV-Gad1-mCherry. Following smSDS exposure, mice injected with AAV-Gad1-mCherry showed a significant reduction in SI time (Fig. 5H), whereas mice injected with AAV-Gad1-Cartpt showed a SI time that was comparable to that of non-stressed animals (Fig. 5I). These results suggest that CART peptide induction in the GABAergic neurons of the aCC drives antidepressant-like behavior and stress resilience independently of genetic background.

Antidepressant-like effect of CART peptide induction in an animal model of stress-induced depression

Because CART peptide induction before and during stress episodes prevented stress-induced depression-like behaviors (Figs 4 and 5), we tested whether CART peptide overexpression after stress induction reversed depression-like behaviors. We used a tetracycline system to overexpress CART peptides after the termination of CSDS episodes. We injected a cocktail of AAVs expressing a tetracycline-dependent transcription activator (Tet3G) under the control of the

SynI promoter (AAV-SynI-tet3G-2A-mCherry^{nls}), together with a Cre- and tetracycline-dependent AAV expressing CART peptide and EGFP (AAV-TRE-FLEX-Cartpt-2A-EGFP) and an AAV expressing a tetracycline-dependent transcription silencer (AAV-CMV-tTS), into the aCC of vGat-Cre mice (Fig. 6A). In this system, tTS represses TRE-mediated gene expression (i.e., *Cartpt* and *Egfp*) in the absence of Dox, whereas in the presence of Dox, Tet3G activates TRE-mediated gene expression specifically in Cre-expressing Gad1 neurons (Fig. 6B). For verification, we performed histological analysis; a GFP signal was observed in mCherry-positive neurons in a Dox-dependent manner (Fig. 6C). We then subjected AAV-injected mice to CSDS, performed SIT (SIT-1), and classified them as susceptible (SUS) and resilient (RES) mice (Fig. 6D) based on their SI ratio with a cutoff value: mice with an SI ratio of <1 were labeled as SUS and those with an SI ratio of >1 as RES, as reported previously (24) (Fig. 6E). After CSDS exposure, SUS and non-stressed mice were treated with Dox for 3 days to induce transgene expression, followed by SIT (SIT-2) (Fig. 6D). We found that CART peptide induction by dox treatment in the SUS mice after CSDS episodes showed significantly increased SI time in SIT-2, when compared to saline-treated SUS mice (Fig. 6F). These data suggest that CART peptide induction in Gad1 neurons of the aCC is sufficient for inducing the antidepressant response.

Discussion

Investigating antidepressant-induced transcriptional changes in responders and nonresponders can help distinguish drug-induced therapeutic changes from off-target effects (16, 36). We found fundamental differences in the transcription signatures of antidepressant responders and nonresponders. In addition to the individual differences within a given genetic background, it is known that phenotypic responses often vary depending on genetic backgrounds (37) and that the genetic background influences a behavioral response to antidepressants in mice (17-19). Although responses to antidepressants in clinical depression vary (1), a limited number of preclinical studies have

mentioned the issue of heterogeneity observed in antidepressant responses (16, 36). Herein, we used an experimental strategy to identify a specific molecule responsible for antidepressant responses among multiple antidepressant drugs that is independent of genetic background; this approach may be informative in terms of translational research and drug development. We identified the CART peptide as a common molecule underlying the antidepressant response, suggesting that it is a strong candidate for anti-depression treatment.

We investigated whether a common set of genes is regulated in the same way in BALB mice treated with two classes of antidepressants (i.e., SSRI and SNRI). Most of the regulated genes differed between these classes and between responders and nonresponders. Only seven genes, including immediate early genes (*c-fos*, *Egr1*, and *Egr2*), were consistently upregulated in responders and nonresponders to SRT and DLX (Fig. 2B). Because enhanced immediate early gene expression is thought to be associated with high neuronal activity, our data suggest that certain cell populations within the mPFC respond to antidepressants regardless of behavioral alterations.

We found that, unlike the expression of immediate early genes, *Cartpt* is a common gene upregulated in antidepressant responders of multiple strains and different types of antidepressants. Thus, *Cartpt* expression could be a molecular marker for antidepressant-like behavioral effects, instead of *c-fos* expression, at least in the aCC region. CART peptides are implicated in a wide range of physiological and behavioral functions, including stress response, appetite, sexual behavior, sleep, reward, autonomic regulation, and endocrine control (38-41). Deficits in these functions are often associated with depression symptoms, suggesting the key role played by CART peptides in depression. In humans, a small cohort with the Leu34Phe missense mutation in *CARTPT*, which leads to CART peptide deficiency (42), exhibited higher anxiety and depression scores (43). In rodents, exposure to chronic mild stress was associated with downregulation of *Cartpt* mRNA expression in the frontal cortex (44), and the electroconvulsive stimulation, used for treatment-resistant depression, upregulated *Cartpt* mRNA and protein expression in the nucleus

accumbens of rats (45). Our study provides previously missing, precise, and cell-type specific roles of CART peptides in behavioral regulation, such as anxiety, social interaction, active escape behavior, and anhedonia, in response to antidepressant treatment. Thus, CART peptide could be, at least in the aCC area, an endogenous antidepressant.

Our data indicated that the expression of *Cartpt* was increased in the aCC of antidepressant responder mice and that the aCC-specific overexpression of CART peptide promoted antidepressant-like behavioral response, suggesting a possible contribution of aCC to the behavioral response to antidepressants. It is important to compare homologous sites in order to synthesize the findings in rodents and humans, but the most commonly used partitioning of the rodent aCC is inconsistent with that of humans (46). In addition, there is a discrepancy in the cross-species definition of the aCC (46-48). Nevertheless, the site we have targeted in this study (corresponding to the anterior part of Brodmann area 24 in humans) can be regarded as the ACC by any definitions. Multiple clinical studies have suggested that the ACC is involved in the pathophysiology of depression (49-52). Preclinical studies also revealed that structural plasticity within the aCC plays a critical role in the rapid antidepressant-like behavior afforded by ketamine and psilocybin (13, 53). These results support our notion that aCC function could be associated with promoting behavioral responses to antidepressants and stress resiliency.

We also identified a GABAergic neuron-specific role of CART peptides in antidepressant effects. The involvement of PFC GABA-related genes has been suggested in MDD pathophysiology (8, 9, 54), supporting a recent single-nucleus transcriptomics analysis of the postmortem PFC in MDD, which suggests that cortical neuron subtypes are involved in depression (10). Enhanced cortical GABA levels in MDD could be a potential mechanism underlying the treatment effects of typical antidepressants, ketamine, rTMS, and ECT (55-58). Preclinical studies have demonstrated that the regulation of depression-related and antidepressant-like behaviors depends on the interneuron subtype targeted within the mPFC and/or aCC (59-61). Thus,

abundant evidence supports the notion that the cortical GABAergic system is a key regulator of stress-induced behavioral changes and antidepressant-like behaviors. Although how CART peptides modulate GABA neurotransmission in the aCC remains unknown, the interaction between CART peptides and GABA signals might provide critical clues regarding the mechanism of action of antidepressants.

This study has several limitations. We used only male mice; therefore, our results are not necessarily generalizable to females. Given that previous evidence suggests sex-specific transcriptome changes in MDD and differences in antidepressant responsiveness between genders (62-64), further studies are necessary. Nonetheless, our study provides important information for subsequent studies aimed at exploring both male and female antidepressant responders. We found individual *Cartpt* expression differences in the antidepressant treatment response, whereas the underlying mechanisms remain unclear. Although a genetic component might account for the antidepressant response (20, 65), it has been suggested that MDD and treatment responses result from genetic and environmental interactions. Such interactions could be mediated by epigenetic mechanisms and we speculate that differential epigenetic marks on the *Cartpt* gene, along with environmental and genetic factors, might influence its transcription and determine the behavioral response to antidepressants. Future work would be required to delineate the relative contribution of epigenetic, genetic, and environmental factors that might explain together the variations in the role the antidepressants play. It will also be important to determine how the CART peptide-dependent signal exerts antidepressant-like behaviors. These studies remained limited by absence of any identified CART peptide receptors. However, recent reports have identified two orphan receptors, GPR68 and GPR160, as putative receptors for CART peptides (66, 67). Although it remains unclear whether CART peptides can stimulate these GPRs in the brain, understanding these receptors, their interaction with CART peptides, and their roles in mood and emotion may provide novel insights for the treatment of psychiatric disorders.

In conclusion, our data suggest that CART peptide signaling in GABAergic neurons of the aCC might be a common molecular mechanism across antidepressant responders independent of genetic backgrounds, and that this pathway also drives stress resilience. This study may provide a strategy for identifying novel drug targets and developing approaches that positively modulate CART peptide signaling represents a promising avenue for treating depression.

Acknowledgments

We thank Mr. Naoto Yasuda, Ms. Ayumi Kobayashi, Ms. Kaede Kuroda, and Ms. Kumiko Hara for technical assistance.

Author Contribution

Y.F., N.O., and S.U. designed the study. Y.F., H.L., A.K., E.I., H.I., H.Y., T.S., and S.U. performed the experiments. N.O and S.U. analyzed RNA-seq data. S.N. and Y.W. provided critical reagents. Y.F., N.O., and S.U. wrote the manuscript with input from T.M.

Funding

This work was supported by JSPS KAKENHI grant numbers JP18H02750, JP21K19707, JP21H02849, JP21K15711, and JP21K07593, by MEXT KAKENHI grant number JP21H00198, and by AMED under grant numbers JP20ak0101136 and JP21dm0307102h0003.

Conflict of Interest Statement

The authors report no biomedical financial interests or potential conflicts of interest.

References

1. Rush AJ, Trivedi MH, Wisniewski SR, Nierenberg AA, Stewart JW, Warden D, et al. (2006): Acute and longer-term outcomes in depressed outpatients requiring one or several treatment steps: a STAR*D report. *Am J Psychiatry*. 163:1905-1917.

2. Pizzagalli DA, Roberts AC (2021): Prefrontal cortex and depression. *Neuropsychopharmacology*.

3. Ploski JE, Vaidya VA (2021): The Neurocircuitry of Posttraumatic Stress Disorder and Major Depression: Insights Into Overlapping and Distinct Circuit Dysfunction-A Tribute to Ron Duman. *Biol Psychiatry*. 90:109-117.

4. Krishnan V, Nestler EJ (2010): Linking molecules to mood: new insight into the biology of depression. *Am J Psychiatry*. 167:1305-1320.

5. Drevets WC (2000): Functional anatomical abnormalities in limbic and prefrontal cortical structures in major depression. *Prog Brain Res*. 126:413-431.

6. Mayberg HS, Liotti M, Brannan SK, McGinnis S, Mahurin RK, Jerabek PA, et al. (1999): Reciprocal limbic-cortical function and negative mood: converging PET findings in depression and normal sadness. *Am J Psychiatry*. 156:675-682.

7. Duman RS, Aghajanian GK (2012): Synaptic dysfunction in depression: potential therapeutic targets. *Science*. 338:68-72.

8. Girgenti MJ, Wang J, Ji D, Cruz DA, Traumatic Stress Brain Research G, Stein MB, et al. (2021): Transcriptomic organization of the human brain in post-traumatic stress disorder. *Nat Neurosci*. 24:24-33.

9. Sequeira A, Mamdani F, Ernst C, Vawter MP, Bunney WE, Lebel V, et al. (2009): Global brain gene expression analysis links glutamatergic and GABAergic alterations to suicide and major depression. *PLoS One*. 4:e6585.

10. Nagy C, Maitra M, Tanti A, Suderman M, Theroux JF, Davoli MA, et al. (2020): Single-nucleus transcriptomics of the prefrontal cortex in major depressive disorder implicates oligodendrocyte precursor cells and excitatory neurons. *Nat Neurosci*. 23:771-781.

11. Duman RS, Sanacora G, Krystal JH (2019): Altered Connectivity in Depression: GABA and Glutamate Neurotransmitter Deficits and Reversal by Novel Treatments. *Neuron*. 102:75-90.

12. Covington HE, 3rd, Lobo MK, Maze I, Vialou V, Hyman JM, Zaman S, et al. (2010): Antidepressant effect of optogenetic stimulation of the medial prefrontal cortex. *J Neurosci*. 30:16082-16090.

13. Moda-Sava RN, Murdock MH, Parekh PK, Fetcho RN, Huang BS, Huynh TN, et al. (2019): Sustained rescue of prefrontal circuit dysfunction by antidepressant-induced spine formation. *Science*. 364.
14. Ferenczi EA, Zalocusky KA, Liston C, Grosenick L, Warden MR, Amatya D, et al. (2016): Prefrontal cortical regulation of brainwide circuit dynamics and reward-related behavior. *Science*. 351:aac9698.
15. Uchida S, Hara K, Kobayashi A, Funato H, Hobara T, Otsuki K, et al. (2010): Early life stress enhances behavioral vulnerability to stress through the activation of REST4-mediated gene transcription in the medial prefrontal cortex of rodents. *J Neurosci*. 30:15007-15018.
16. Bagot RC, Cates HM, Purushothaman I, Vialou V, Heller EA, Yieh L, et al. (2017): Ketamine and Imipramine Reverse Transcriptional Signatures of Susceptibility and Induce Resilience-Specific Gene Expression Profiles. *Biol Psychiatry*. 81:285-295.
17. Dulawa SC, Holick KA, Gundersen B, Hen R (2004): Effects of chronic fluoxetine in animal models of anxiety and depression. *Neuropsychopharmacology*. 29:1321-1330.
18. Schmidt EF, Warner-Schmidt JL, Otopalik BG, Pickett SB, Greengard P, Heintz N (2012): Identification of the cortical neurons that mediate antidepressant responses. *Cell*. 149:1152-1163.
19. Crowley JJ, Brodkin ES, Blendy JA, Berrettini WH, Lucki I (2006): Pharmacogenomic evaluation of the antidepressant citalopram in the mouse tail suspension test. *Neuropsychopharmacology*. 31:2433-2442.
20. Santarelli L, Saxe M, Gross C, Surget A, Battaglia F, Dulawa S, et al. (2003): Requirement of hippocampal neurogenesis for the behavioral effects of antidepressants. *Science*. 301:805-809.
21. Uchida S, Hara K, Kobayashi A, Otsuki K, Yamagata H, Hobara T, et al. (2011): Epigenetic status of Gdnf in the ventral striatum determines susceptibility and adaptation to daily stressful events. *Neuron*. 69:359-372.
22. Golden SA, Covington HE, 3rd, Berton O, Russo SJ (2011): A standardized protocol for repeated social defeat stress in mice. *Nat Protoc*. 6:1183-1191.
23. Sakai Y, Li H, Inaba H, Funayama Y, Ishimori E, Kawatake-Kuno A, et al. (2021): Gene-environment interactions mediate stress susceptibility and resilience through the CaMKIIbeta/TARPgamma-8/AMPAR pathway. *iScience*. 24:102504.

24. Krishnan V, Han MH, Graham DL, Berton O, Renthal W, Russo SJ, et al. (2007): Molecular adaptations underlying susceptibility and resistance to social defeat in brain reward regions. *Cell*. 131:391-404.
25. Uchida S, Hara K, Kobayashi A, Fujimoto M, Otsuki K, Yamagata H, et al. (2011): Impaired hippocampal spinogenesis and neurogenesis and altered affective behavior in mice lacking heat shock factor 1. *Proc Natl Acad Sci U S A*. 108:1681-1686.
26. Zanos P, Moaddel R, Morris PJ, Georgiou P, Fischell J, Elmer GI, et al. (2016): NMDAR inhibition-independent antidepressant actions of ketamine metabolites. *Nature*. 533:481-486.
27. Casarotto PC, Girych M, Fred SM, Kovaleva V, Moliner R, Enkavi G, et al. (2021): Antidepressant drugs act by directly binding to TRKB neurotrophin receptors. *Cell*. 184:1299-1313 e1219.
28. Porsolt RD, Le Pichon M, Jalfre M (1977): Depression: a new animal model sensitive to antidepressant treatments. *Nature*. 266:730-732.
29. David DJ, Samuels BA, Rainer Q, Wang JW, Marsteller D, Mendez I, et al. (2009): Neurogenesis-dependent and -independent effects of fluoxetine in an animal model of anxiety/depression. *Neuron*. 62:479-493.
30. Trivedi MH, Rush AJ, Wisniewski SR, Nierenberg AA, Warden D, Ritz L, et al. (2006): Evaluation of outcomes with citalopram for depression using measurement-based care in STAR*D: implications for clinical practice. *Am J Psychiatry*. 163:28-40.
31. Laine MA, Trontti K, Misiewicz Z, Sokolowska E, Kulesskaya N, Heikkinen A, et al. (2018): Genetic Control of Myelin Plasticity after Chronic Psychosocial Stress. *eNeuro*. 5.
32. Luo Y, Kataoka Y, Ostinelli EG, Cipriani A, Furukawa TA (2020): National Prescription Patterns of Antidepressants in the Treatment of Adults With Major Depression in the US Between 1996 and 2015: A Population Representative Survey Based Analysis. *Front Psychiatry*. 11:35.
33. Yu Z, Zhang J, Zheng Y, Yu L (2020): Trends in Antidepressant Use and Expenditure in Six Major Cities in China From 2013 to 2018. *Front Psychiatry*. 11:551.
34. Doyle JP, Dougherty JD, Heiman M, Schmidt EF, Stevens TR, Ma G, et al. (2008): Application of a translational profiling approach for the comparative analysis of CNS cell types. *Cell*. 135:749-762.
35. Heiman M, Schaefer A, Gong S, Peterson JD, Day M, Ramsey KE, et al.

(2008): A translational profiling approach for the molecular characterization of CNS cell types. *Cell*. 135:738-748.

36. Carrillo-Roa T, Labermaier C, Weber P, Herzog DP, Lareau C, Santarelli S, et al. (2017): Common genes associated with antidepressant response in mouse and man identify key role of glucocorticoid receptor sensitivity. *PLoS Biol*. 15:e2002690.

37. Sittig LJ, Carbonetto P, Engel KA, Krauss KS, Barrios-Camacho CM, Palmer AA (2016): Genetic Background Limits Generalizability of Genotype-Phenotype Relationships. *Neuron*. 91:1253-1259.

38. Rogge G, Jones D, Hubert GW, Lin Y, Kuhar MJ (2008): CART peptides: regulators of body weight, reward and other functions. *Nat Rev Neurosci*. 9:747-758.

39. Lau J, Herzog H (2014): CART in the regulation of appetite and energy homeostasis. *Front Neurosci*. 8:313.

40. Singh A, de Araujo AM, Krieger JP, Vergara M, Ip CK, de Lartigue G (2021): Demystifying functional role of cocaine- and amphetamine-related transcript (CART) peptide in control of energy homeostasis: A twenty-five year expedition. *Peptides*. 140:170534.

41. Ahmadian-Moghadam H, Sadat-Shirazi MS, Zarrindast MR (2018): Cocaine- and amphetamine-regulated transcript (CART): A multifaceted neuropeptide. *Peptides*. 110:56-77.

42. Yanik T, Dominguez G, Kuhar MJ, Del Giudice EM, Loh YP (2006): The Leu34Phe ProCART mutation leads to cocaine- and amphetamine-regulated transcript (CART) deficiency: a possible cause for obesity in humans. *Endocrinology*. 147:39-43.

43. Miraglia del Giudice E, Santoro N, Fiumani P, Dominguez G, Kuhar MJ, Perrone L (2006): Adolescents carrying a missense mutation in the CART gene exhibit increased anxiety and depression. *Depress Anxiety*. 23:90-92.

44. Orsetti M, Di Brisco F, Canonico PL, Genazzani AA, Ghi P (2008): Gene regulation in the frontal cortex of rats exposed to the chronic mild stress paradigm, an animal model of human depression. *Eur J Neurosci*. 27:2156-2164.

45. Roh MS, Cui FJ, Ahn YM, Kang UG (2009): Up-regulation of cocaine- and amphetamine-regulated transcript (CART) in the rat nucleus accumbens after repeated electroconvulsive shock. *Neurosci Res*. 65:210-213.

46. van Heukelum S, Mars RB, Guthrie M, Buitelaar JK, Beckmann CF,

Tiesinga PHE, et al. (2020): Where is Cingulate Cortex? A Cross-Species View. *Trends Neurosci*. 43:285-299.

47. Bicks LK, Koike H, Akbarian S, Morishita H (2015): Prefrontal Cortex and Social Cognition in Mouse and Man. *Front Psychol*. 6:1805.

48. Vogt BA, Paxinos G (2014): Cytoarchitecture of mouse and rat cingulate cortex with human homologies. *Brain Struct Funct*. 219:185-192.

49. Goldapple K, Segal Z, Garson C, Lau M, Bieling P, Kennedy S, et al. (2004): Modulation of cortical-limbic pathways in major depression: treatment-specific effects of cognitive behavior therapy. *Arch Gen Psychiatry*. 61:34-41.

50. Goodman M, Hazlett EA, Avedon JB, Siever DR, Chu KW, New AS (2011): Anterior cingulate volume reduction in adolescents with borderline personality disorder and co-morbid major depression. *J Psychiatr Res*. 45:803-807.

51. Youssef MM, Underwood MD, Huang YY, Hsiung SC, Liu Y, Simpson NR, et al. (2018): Association of BDNF Val66Met Polymorphism and Brain BDNF Levels with Major Depression and Suicide. *Int J Neuropsychopharmacol*. 21:528-538.

52. Gibbons A, McPherson K, Gogos A, Dean B (2021): An investigation into nicotinic receptor involvement in mood disorders uncovers novel depression candidate genes. *J Affect Disord*. 288:154-160.

53. Shao LX, Liao C, Gregg I, Davoudian PA, Savalia NK, Delagarza K, et al. (2021): Psilocybin induces rapid and persistent growth of dendritic spines in frontal cortex in vivo. *Neuron*. 109:2535-2544 e2534.

54. Northoff G, Sibille E (2014): Why are cortical GABA neurons relevant to internal focus in depression? A cross-level model linking cellular, biochemical and neural network findings. *Mol Psychiatry*. 19:966-977.

55. Sanacora G, Mason GF, Rothman DL, Krystal JH (2002): Increased occipital cortex GABA concentrations in depressed patients after therapy with selective serotonin reuptake inhibitors. *Am J Psychiatry*. 159:663-665.

56. Sanacora G, Mason GF, Rothman DL, Hyder F, Ciarcia JJ, Ostroff RB, et al. (2003): Increased cortical GABA concentrations in depressed patients receiving ECT. *Am J Psychiatry*. 160:577-579.

57. Dubin MJ, Mao X, Banerjee S, Goodman Z, Lapidus KA, Kang G, et al. (2016): Elevated prefrontal cortex GABA in patients with major depressive disorder after TMS treatment measured with proton magnetic resonance spectroscopy. *J Psychiatry Neurosci*. 41:E37-45.

58. Milak MS, Proper CJ, Mulhern ST, Parter AL, Kegeles LS, Ogden RT, et al. (2016): A pilot in vivo proton magnetic resonance spectroscopy study of amino acid neurotransmitter response to ketamine treatment of major depressive disorder. *Mol Psychiatry*. 21:320-327.

59. Fogaca MV, Wu M, Li C, Li XY, Picciotto MR, Duman RS (2020): Inhibition of GABA interneurons in the mPFC is sufficient and necessary for rapid antidepressant responses. *Mol Psychiatry*.

60. Fuchs T, Jefferson SJ, Hooper A, Yee PH, Maguire J, Luscher B (2017): Disinhibition of somatostatin-positive GABAergic interneurons results in an anxiolytic and antidepressant-like brain state. *Mol Psychiatry*. 22:920-930.

61. Perova Z, Delevich K, Li B (2015): Depression of excitatory synapses onto parvalbumin interneurons in the medial prefrontal cortex in susceptibility to stress. *J Neurosci*. 35:3201-3206.

62. Labonte B, Engmann O, Purushothaman I, Menard C, Wang J, Tan C, et al. (2017): Sex-specific transcriptional signatures in human depression. *Nat Med*. 23:1102-1111.

63. Kawatake-Kuno A, Murai T, Uchida S (2021): The Molecular Basis of Depression: Implications of Sex-Related Differences in Epigenetic Regulation. *Front Mol Neurosci*. 14:708004.

64. Kornstein SG, Schatzberg AF, Thase ME, Yonkers KA, McCullough JP, Keitner GI, et al. (2000): Gender differences in treatment response to sertraline versus imipramine in chronic depression. *Am J Psychiatry*. 157:1445-1452.

65. Uhr M, Tontsch A, Namendorf C, Ripke S, Lucae S, Ising M, et al. (2008): Polymorphisms in the drug transporter gene ABCB1 predict antidepressant treatment response in depression. *Neuron*. 57:203-209.

66. Foster SR, Hauser AS, Vedel L, Strachan RT, Huang XP, Gavin AC, et al. (2019): Discovery of Human Signaling Systems: Pairing Peptides to G Protein-Coupled Receptors. *Cell*. 179:895-908 e821.

67. Yosten GL, Harada CM, Haddock C, Giancotti LA, Kolar GR, Patel R, et al. (2020): GPR160 de-orphanization reveals critical roles in neuropathic pain in rodents. *J Clin Invest*. 130:2587-2592.

Figure 1. Identification of subgroups of responders and nonresponders to antidepressant treatments in inbred strains of mice.

A. Experimental design. Mice were tested using the forced swim test (FST-1) prior to a 3-week treatment with either tap water (V), imipramine (IMI), maprotiline (MPR), sertraline (SRT), or duloxetine (DLX). After the chronic treatment with the antidepressant, a second forced swim test (FST-2) was performed.

B–D. Immobility time in the FST-2 (% FST-1) in BALB (B), B6 (C), and DBA (D) mice. n = 36–40 in each group. *p < 0.05 vs. FST-1 in the corresponding treatment.

E–G. Response ratio (immobility time in FST-1 / immobility time in FST-2). The responder and nonresponder subgroups were identified by the mean + 2SD method with a cutoff value. n = 36–40 in each group.

H. Distribution of responders and nonresponders in each strain of mice treated with specific antidepressants. n = 36–40 in each group.

All data are presented as the mean ± SEM.

Figure 2. RNA-seq reveals transcriptional alterations in the mPFC of antidepressant responders and nonresponders.

A. Heatmap representation of differentially expressed genes (fold change >1.3 and FDR P <0.1) in the responder and nonresponder groups to treatment with sertraline (SRT) and duloxetine (DLX) (three replicates per group).

B. Heatmap representation of differentially expressed genes (fold change >1.3 and FDR P <0.1) that were commonly upregulated in both responders and nonresponders to treatment with SRT and DLX.

C–I. Real-time PCR validation of the alterations in gene expression identified in the differentially expressed gene analysis presented in B. n = 6 in each group. *Adjusted p < 0.05 vs. the vehicle.

J–M. MA plot of the results of the differential expression analysis in SRT-responders (J), SRT-nonresponders (K), DLX-responders (L), or DLX-

nonresponders (M).

N. GO profile analysis (biological process) of differentially expressed genes (P < 0.05) between the vehicle and SRT-responders, SRT-nonresponders, DLX-responders, or DLX-nonresponders (red, upregulated genes; blue, downregulated genes). The X-axis displays the number of differentially expressed genes and the Y-axis indicates the GO terms.

All data are presented as the mean ± SEM.

Figure 3. Identification of *Cartpt* consistent upregulation across different types of antidepressant responders in three strains of mice.

A. Venn diagram indicating the number of differentially expressed genes across four comparisons (SRT-responders, SRT-nonresponders, DLX-responders, DLX-nonresponders) and the overlap between the sets of genes.

B. Heatmap showing the 68 differentially regulated genes (fold change >1.3 and P < 0.05) that were consistently regulated in SRT and DLX treatment responders, but not in SRT or DLX treatment nonresponders.

C–F. GO enrichment analysis (C and E) and network graph visualization (D and F) of differentially expressed genes that were regulated in SRT (C and D) and DLX (E and F) treatment responders. Top-five significant GO terms associated with differentially expressed genes in SRT-R and DLX-R. Note that the significant GO terms are associated with the neuropeptide signaling pathway (i.e., *Cartpt*) in responders to both antidepressant treatments.

G-I. Q-PCR revealing the upregulation of *Cartpt* in the mPFC of IMI-, MPR-, SRT-, and DLX-responders, but not in their nonresponder counterparts in BALB (G), B6 (H), and DBA (I) mice. n = 4–6 in each group. *Adjusted p < 0.05 vs. the vehicle.

J. TRAP strategy. EGFP-labeled polysomes were affinity-purified to enrich for glutamatergic or GABAergic neuron-specific, polysome-bound, translating mRNAs.

K and L. Q-PCR quantification of *Cartpt* expression in vGat-TRAP (K) and vGlut-TRAP (L) samples (relative to the vehicle). n = 4–5 samples in each

group, and each sample was pooled from 4–6 mice (8–10 pairs of mPFC). * Adjusted $p < 0.05$.

M. RNAscope revealing that *Cartpt* expression (green) was enriched in the *Slc32a1*+ GABAergic neurons (magenta), but not in the *Camk2a*+ glutamatergic neurons (red) in the anterior cingulate cortex (Cg1/Cg2) of mice. The arrowheads and arrows indicate *Slc32a1*+ GABAergic neurons and *Camk2a*+ glutamatergic neurons, respectively. Scale bar, 100 μm.

All data are presented as the mean ± SEM.

Figure 4. CART peptides in GABAergic neurons of the aCC drive antidepressant-like behaviors and stress resilience.

A. AAV vectors used for the control construct (AAV-tdTomato) and *Cartpt* overexpression (AAV-Cartpt).

B. Experimental paradigm of behavioral testing. CSDS, chronic social defeat stress; FST, forced swim test; SIT, social interaction test; SPT, sucrose preference test; OFT, open field test; NS, non-stress control.

C. AAV microinjection into the aCC. Region-specific expression of tdTomato in the aCC is shown. Scale bar, 100 μm.

D–G. Effects of *Cartpt* overexpression in GABAergic neurons of the aCC on the FST (D), SIT (E), SPT (F), and OFT (G). n = 23–24 for FST and n = 11–13 for SIT, SPT, and OFT in each group. *$p < 0.05$.

H–K. Effects of *Cartpt* overexpression in glutamatergic neurons of the aCC on the FST (H), SIT (I), SPT (J), and OFT (K). n = 23–24 for the FST and n = 11–14 for the SIT, SPT, and OFT in each group. *$p < 0.05$.

All data are presented as the mean ± SEM.

Figure 5. AAV-mediated CART peptide overexpression in aCC GABAergic neurons drives antidepressant-like behaviors and stress resilience in stress-vulnerable strains.

A. AAV vectors used for *mCherry* overexpression under the control of the *Gad1* promoter (AAV-Gad1-mCherry). To validate the cell-type-specificity of the

Gad1 promoter in these AAVs, AAV-Gad1-mCherry was injected bilaterally into the aCC region of either vGat-Cre::GFP-L10a or vGlut-Cre::GFP-L10a mice (as reporter mice).

B. Fluorescence signals of EGFP (green) and mCherry (red) in the aCC of vGat-Cre::GFP-L10a mice (top panels) and vGlut-Cre::GFP-L10a mice (bottom panels). Co-localization of EGFP and mCherry is seen in vGat-Cre::GFP-L10a, but not in vGlut-Cre::GFP-L10a mice. Scale bar, 100 μm.

C. Quantification of the percentage of mCherry-positive cells (red) in the aCC region that overlap with GFP-positive cells (green). mCherry expression driven by the *Gad1* promoter is enriched in GFP-positive cells of vGat-Cre::GFP-L10a mice, but not of vGlut-Cre::GFP-L10a mice. n = 4 in each group; 425–685 mCherry-positive cells per group were analyzed.

D. AAV vectors used for *mCherry* (AAV-control) and *Cartpt* (AAV-Cartpt) overexpression under the control of the *Gad1* promoter.

E. Experimental paradigm used for behavioral testing. smSDS, subchronic, and mild social defeat stress; FST, forced swim test; SIT, social interaction test.

F. Mice injected with AAV-Cartpt show reduced immobility time compared with mice injected with AAV-control in the FST. n = 25–27 in each group. *$p < 0.05$.

G. Mice injected with AAV-Cartpt show a comparable social interaction time to that of mice injected with AAV-control in non-stressed conditions. n = 25–27 in each group. *$p < 0.05$.

H and I. The social interaction time of stressed mice injected with AAV-control was significantly lower than that of non-stressed mice injected with AAV-control (H), whereas this reduction was prevented in mice injected with AAV-Cartpt (I). n = 12–16 in each group. *$p < 0.05$.

All data are presented as the mean ± SEM.

Figure 6. CART peptides in GABAergic neurons of the aCC have an antidepressant effect in stress-susceptible mice.

A. AAV-mediated spatiotemporal gene expression strategy using a cocktail of AAV-SynI-Tet3G-2A-mCherry^{nls}, AAV-TRE-FLEX-Cartpt-2A-EGFP, and AAV-

CMV-tTS.

B. Schematic representation of Dox- and Cre-dependent regulation of TRE-mediated gene expression in the inhibitory neurons using both the tetracycline-dependent activator (Tet3G) and repressor (tTS). Without Dox, tTS represses TRE-mediated gene expression, whereas in the presence of Dox, Tet3G activates TRE-mediated gene expression specifically in Cre-expressing cells.

C. AAV microinjection into the aCC region of vGat-Cre mice. Region-specific and Dox-regulated expression of mCherry in the aCC is shown. Scale bar, 500 μm for low-magnification images (GFP and DAPI) and 50 μm for high-magnification images (GFP and mCherry).

D. Experimental timeline of *Cartpt* induction in inhibitory neurons of the aCC after the termination of CSDS episodes. Mice injected with a cocktail of AAVs were subjected to a 10-day CSDS and were tested by social interaction test (SIT-1), followed by the administration of Dox for 3 days (twice per day). Mice were tested using a social interaction test (SIT-2).

E. Social interaction ratio after CSDS exposure (SIT-1). The CSDS group was divided into two groups [resilience (RES) and susceptible (SUS) groups] based on their SI ratios. n = 32 for NS and 39 for CSDS (both RES and SUS).

F. Social interaction ratio before (SIT-1) and after (SIT-2) Dox administration in NS and SUS mice. CART peptide induction did not affect the social interaction time in non-stressed conditions, whereas the reduced social interaction time in SUS mice was rescued by CART peptide induction with Dox. n = 10–14 in each group. $*p < 0.05$.

All data are presented as the mean ± SEM.

KEY RESOURCES TABLE

Resource Type	Specific Reagent or Resource	Source or Reference	Identifiers	Additional Information
Add additional rows as needed for each resource type	Include species and sex when applicable.	Include name of manufacturer, company, repository, individual, or research lab. Include PMID or DOI for references; use “this paper” if new.	Include catalog numbers, stock numbers, database IDs or accession numbers, and/or RRIDs. RRIDs are highly encouraged; search for RRIDs at https://scicrunch.org/resources.	Include any additional information or notes if necessary.
Organism/Strain	Mouse: C57BL/6J, male	Charles River Japan	RRID: IMSR_JAX:000664	
Organism/Strain	Mouse: BALB/c, male	Charles River Japan	RRID:MGI:6323059	
Organism/Strain	Mouse: DBA/2, male	Charles River Japan	RRID:IMSR_CRL:022	
Organism/Strain	Mouse: CD1, male	Charles River Japan	RRID:IMSR_CRL:026	
Organism/Strain	Mouse: vGlut-Cre, male	Jackson Laboratory	RRID:IMSR_JAX:016963	
Organism/Strain	Mouse: vGat-Cre, male	Jackson Laboratory	RRID:IMSR_JAX:016962	
Organism/Strain	Mouse: EGFP-L10a, male	Jackson Laboratory	RRID:IMSR_JAX:024750	
Chemical Compound or Drug	Imipramine hydrochloride	Tokyo Chemical Industry Co., LTD	I0971	
Chemical Compound or Drug	Maprotiline hydrochloride	Tokyo Chemical Industry Co., LTD	M2527	
Chemical Compound or Drug	Sertraline hydrochloride	Tokyo Chemical Industry Co., LTD	S0507	
Chemical Compound or Drug	Duloxetine hydrochloride	Tokyo Chemical Industry Co., LTD	D4223	
Chemical Compound or Drug	Doxycycline	Sigma	D9891	
Chemical Compound or Drug	Ketamine hydrochloride	Daiichi Sankyo Propharma Co., Ltd	N01AX03	
Commercial Assay Or Kit	DAPI	Sigma	D9542	
Commercial Assay Or Kit	TRIzol Reagent	Thermo Fisher Scientific	15596026	
Commercial Assay Or Kit	Protein G Dynabeads	Thermo Fisher Scientific	10004D	
Commercial Assay Or Kit	SYBR green PCR Master Mix	Thermo Fisher Scientific	4334973	
Commercial Assay Or Kit	Direct-zol RNA Microprep	Zymo research	R2060	
Commercial Assay Or Kit	RNAscope Fluorescent Multiplex 2.0 assay	Advanced Cell Diagnostics	320850	

Key Resource Table

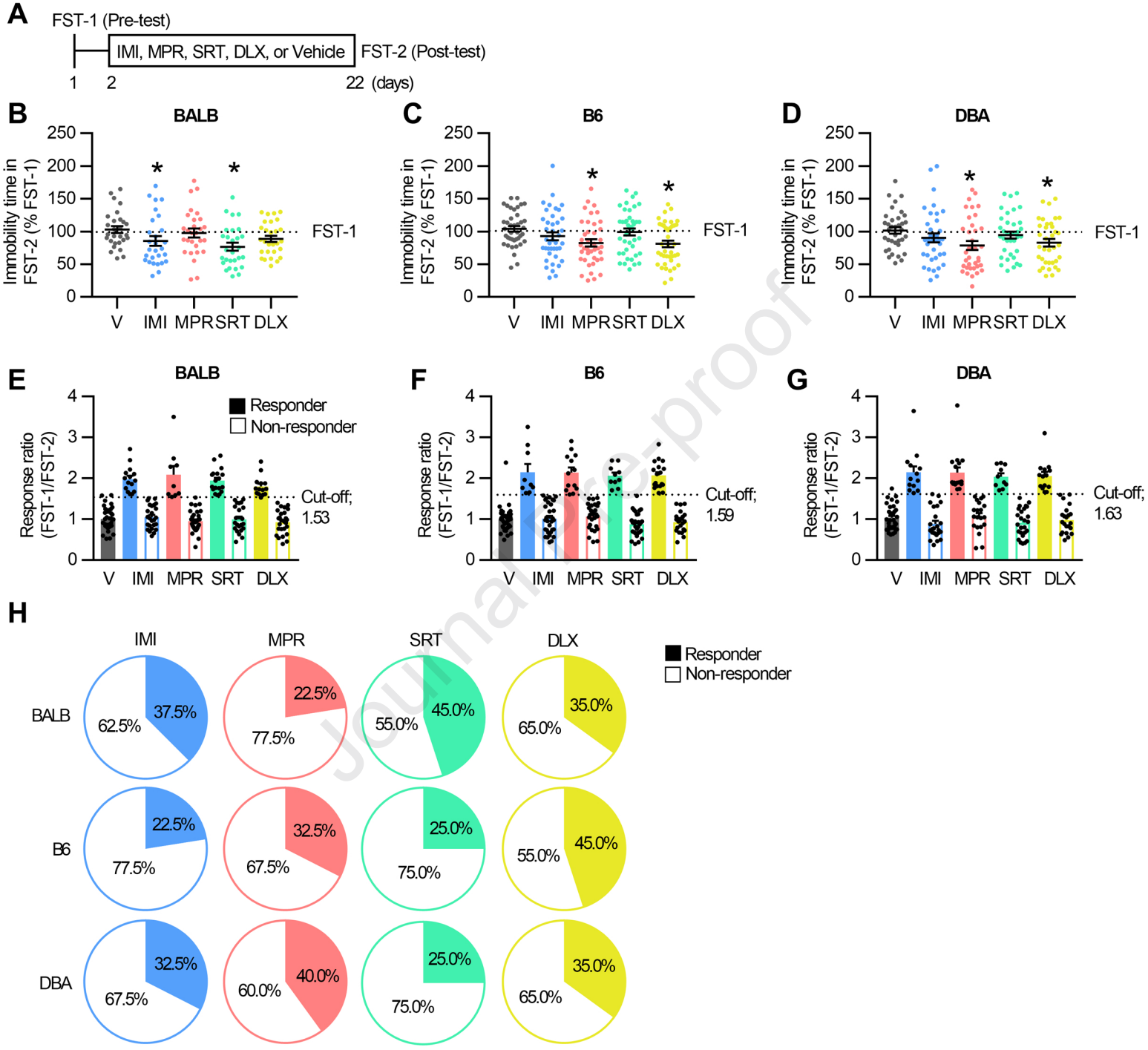

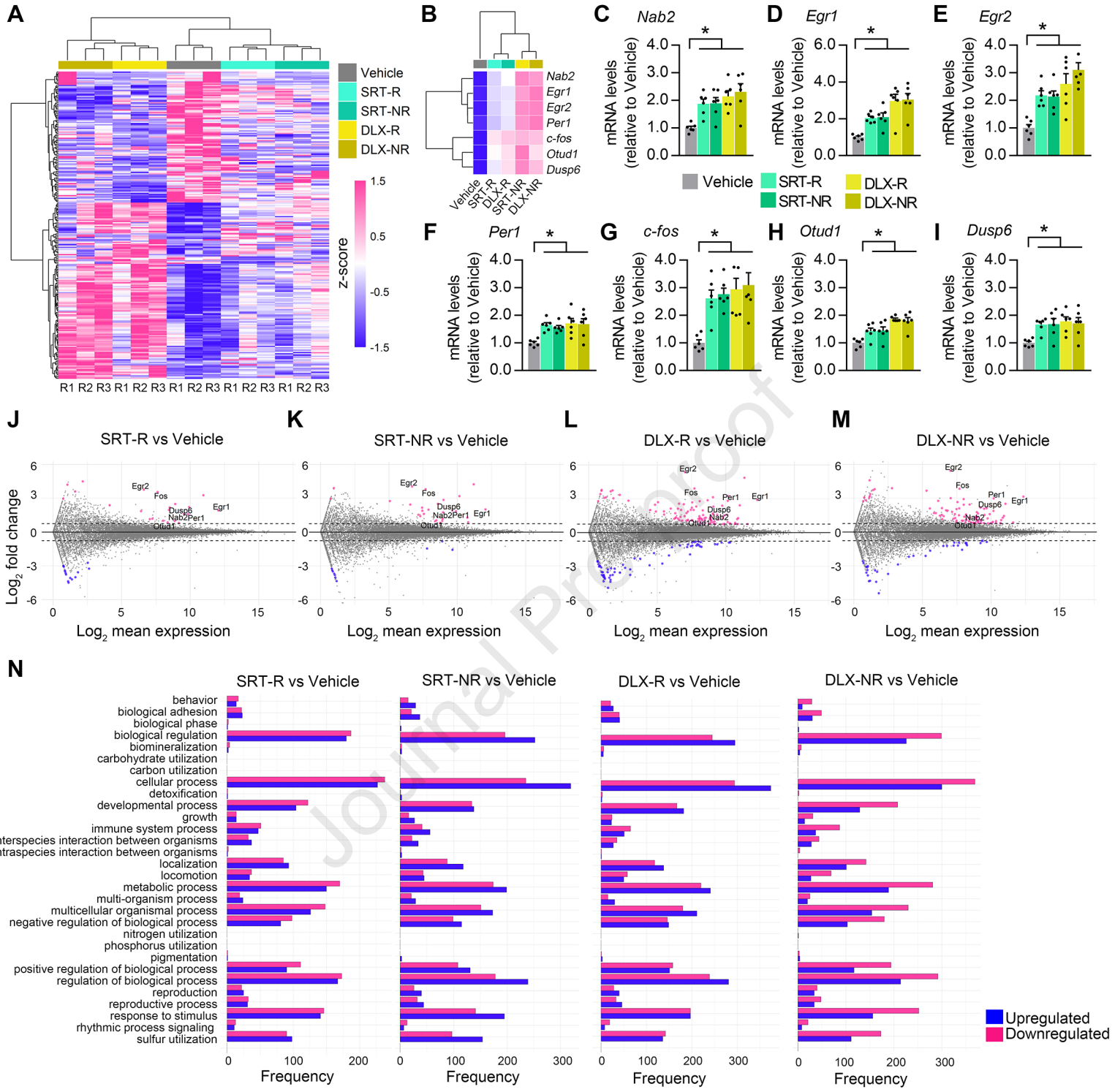

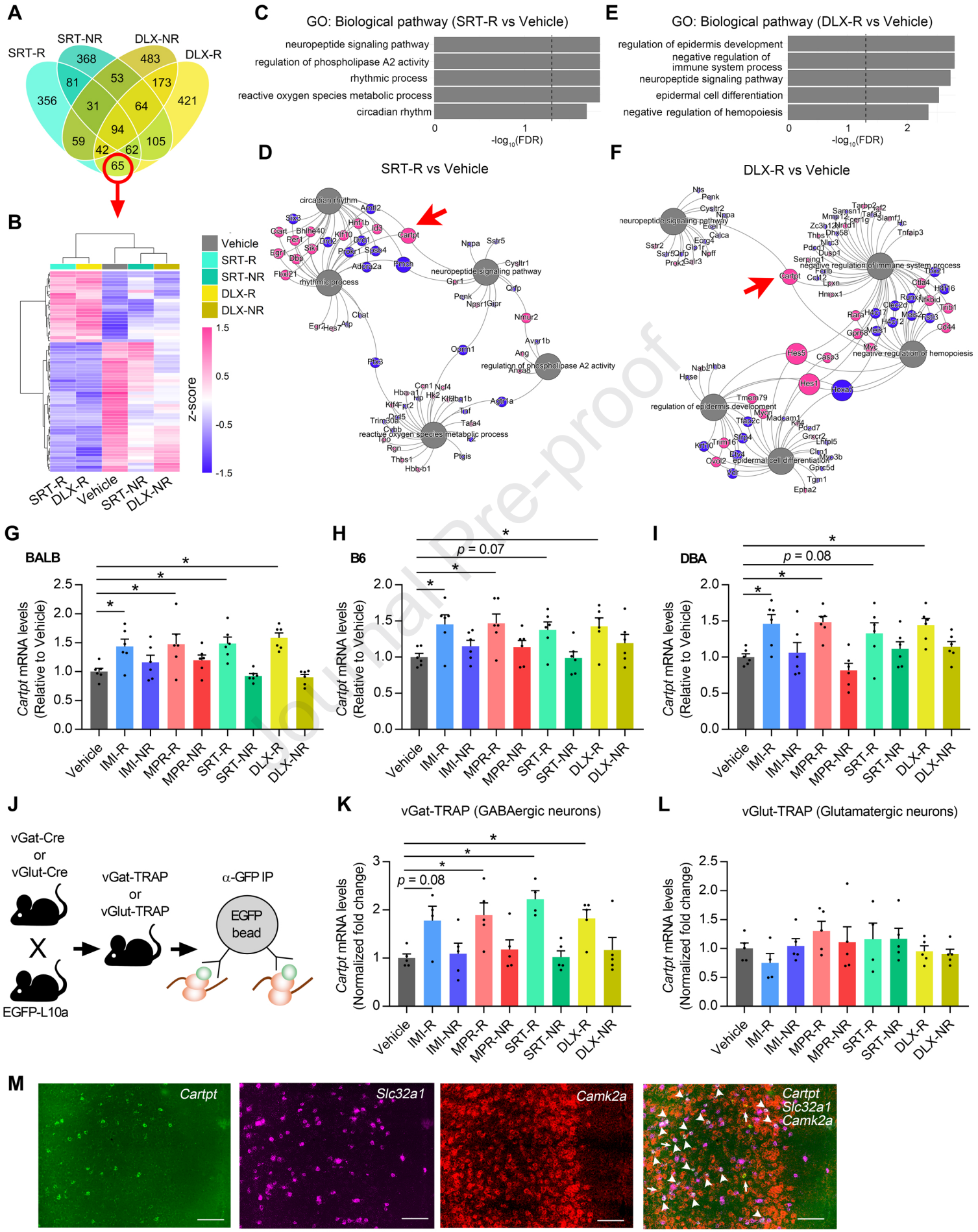

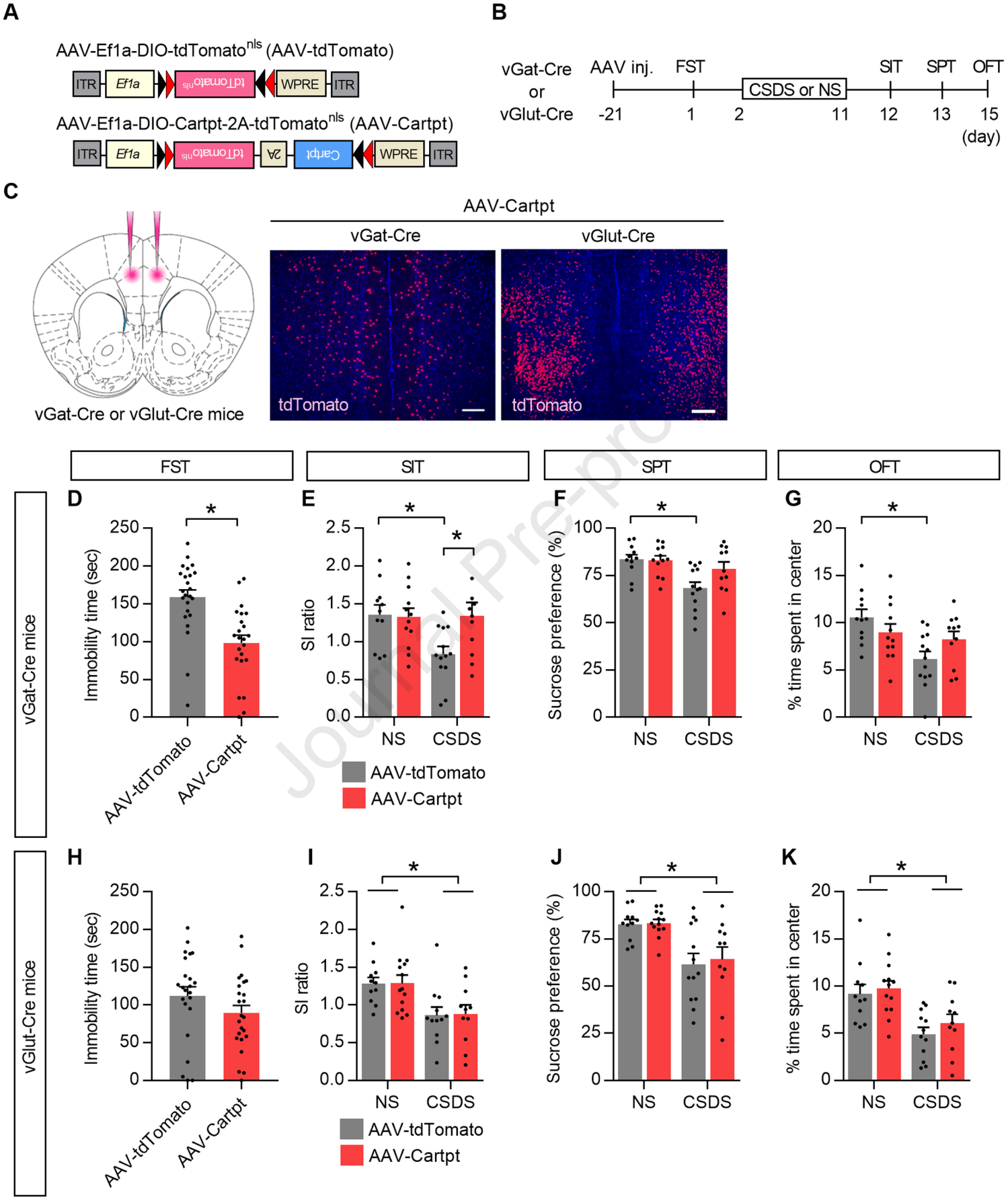

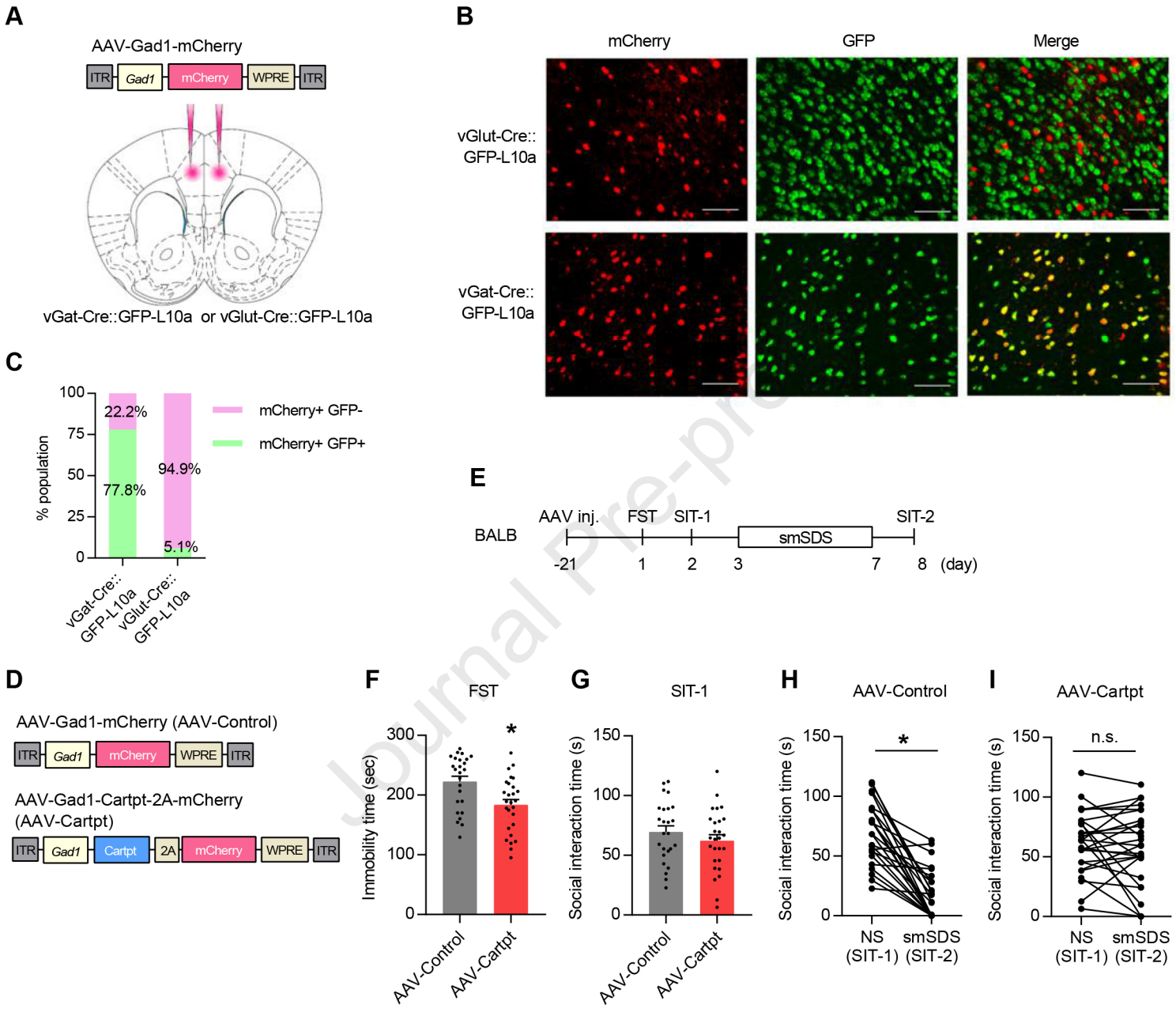
A
AAV-Gad1-mCherry
ITR
Gad1
mCherry
WPRE
ITR
vGat-Cre::GFP-L10a or vGlut-Cre::GFP-L10a
B
mCherry
GFP
Merge
vGlut-Cre::
GFP-L10a
vGat-Cre::
GFP-L10a
C
% population
100
75
50
25
0
22.2%
77.8%
94.9%
5.1%
mCherry+ GFP-
mCherry+ GFP+
vGat-Cre::
GFP-L10a
vGlut-Cre::
GFP-L10a
D
AAV-Gad1-mCherry (AAV-Control)
ITR
Gad1
mCherry
WPRE
ITR
AAV-Gad1-Cartpt-2A-mCherry
(AAV-Cartpt)
ITR
Gad1
Cartpt
2A
mCherry
WPRE
ITR
E
BALB
AAV inj.
FST
SIT-1
smSDS
SIT-2
-21
1
2
3
7
8
(day)
F
FST
Immobility time (sec)
300
200
100
0
*
AAV-Control
AAV-Cartpt
G
SIT-1
Social interaction time (s)
150
100
50
0
AAV-Control
AAV-Cartpt
H
AAV-Control
Social interaction time (s)
150
100
50
0
*
NS
(SIT-1)
smSDS
(SIT-2)
I
AAV-Cartpt
Social interaction time (s)
150
100
50
0
n.s.
NS
(SIT-1)
smSDS
(SIT-2)

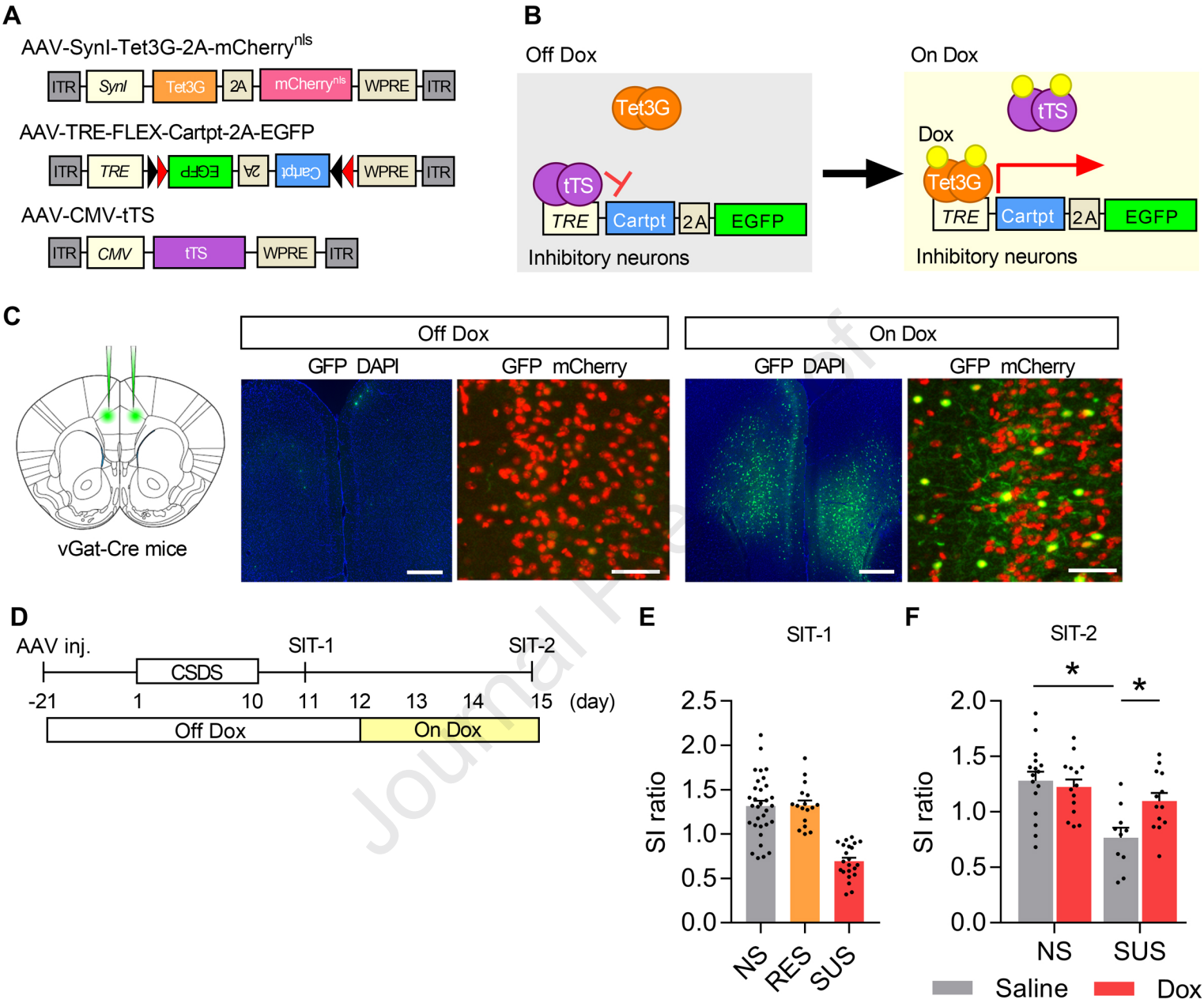
A
AAV-SynI-Tet3G-2A-mCherry^nls
ITR
SynI
Tet3G
2A
mCherry^nls
WPRE
ITR
AAV-TRE-FLEX-Cartpt-2A-EGFP
ITR
TRE
EGFP
2A
Cartpt
WPRE
ITR
AAV-CMV-tTS
ITR
CMV
tTS
WPRE
ITR
B
Off Dox
Tet3G
tTS
TRE
Cartpt
2A
EGFP
Inhibitory neurons
On Dox
tTS
Dox
Tet3G
TRE
Cartpt
2A
EGFP
Inhibitory neurons
C
vGat-Cre mice
Off Dox
GFP DAPI
GFP mCherry
On Dox
GFP DAPI
GFP mCherry
D
AAV inj.
SIT-1
SIT-2
CSDS
-21
1
10
11
12
13
14
15
(day)
Off Dox
On Dox
E
SIT-1
SI ratio
2.5
2.0
1.5
1.0
0.5
0.0
NS
RES
SUS
F
SIT-2
*
*
SI ratio
2.0
1.5
1.0
0.5
0.0
NS
SUS
Saline
Dox

Antidepressant Response and Stress Resilience Are Promoted by CART Peptides in GABAergic Neurons of the Anterior Cingulate Cortex

Supplementary Information

Supplementary Methods

Animals

C57BL/6J, BALB/c, and DBA/2 mice were purchased from Charles River Japan. Retired breeder CD1 male mice were purchased (Charles River) for use as aggressors in the CSDS and smSDS and in the SIT. The vGluT2-IRES::Cre mice (vGlut-Cre mice; JAX stock #016963) or vGat-IRES::Cre mice (vGat-Cre mice; JAX stock #016962) were crossed with Cre-dependent GFP reporter mice (EGFP-L10a mice; JAX stock #024750) to produce vGlut-Cre;EGFP-L10a (vGlut-TRAP) or vGat-Cre;EGFP-L10a (vGat-TRAP) mice, respectively. All data reported in this study were collected from male mice. All mice were housed under a 12-h light/dark cycle (8:00–20:00 light) with food and water available *ad libitum*.

Drug treatment

Imipramine hydrochloride (IMI, Sigma), maprotiline hydrochloride (MPR), sertraline hydrochloride (SRT), and duloxetine hydrochloride (DLX) were purchased from Tokyo Chemical Industry Co., LTD. For continuous treatments, drugs were dissolved in tap water at a concentration of 160 mg/L. This concentration was estimated to achieve a final dose of 16–18 mg/kg/day based on the average amount of water consumed and the average weight of the mice used in this study. Drugs were administered for 3 weeks (chronic) or 5 days (subchronic). Drug solutions were protected from light and were replaced every other day. Control animals received regular drinking water. Ketamine hydrochloride [(*R,S*)-ketamine] (Ketalar; Daiichi Sankyo Propharma Co., Ltd.; Tokyo, Japan) was diluted with saline. Ketamine (20 mg/kg) was administered intraperitoneally (i.p.) into mice. Doxycycline hyclate was purchased from Sigma and administered i.p. (50 mg/kg of body weight, twice per day) to mice.

CSDS

CSDS was performed as previously reported elsewhere and by our group (1, 2). Experimental mice were moved into the home cage of an aggressive CD-1 mouse for 10 min and were physically defeated. After physical interactions, test mice were removed and placed on the opposite side of the perforated divider over the

subsequent 24 h period. For 10 days, experimental mice were exposed to a new resident home cage daily. Control test mice were group housed at four per cage. After the last session, all mice were singly housed and the SIT was conducted.

Subchronic and mild social defeat stress (smSDS)

The smSDS, which is a modified version of the CSDS, was performed as previously reported (2). In this paradigm, BALB/c mice were subjected to defeat stress for a period of five min over five consecutive days, whereas the other procedures were the same as those used in the CSDS condition described above.

Behavioral tests

All behavioral experiments were carried out between 9:00 and 15:00 and were performed in a blinded fashion, as reported previously (2-4).

FST. Mice were gently placed in a cylinder of water (temperature, 24°C ± 1°C; 20 cm in diameter, 15 cm in height). The height of the water was set to prevent mice from touching the bottom of the cylinder with their limbs. Mice were allowed to swim around freely. Each trial lasted for 6 min. Mouse behavior was video-tracked from above and the immobility time was analyzed using an automated software (ANY-maze, Stoelting). In Figure 1B–D, the antidepressant response in the FST-2 was determined as the percentage change in the immobility time from the baseline (FST-1), and the percentage relative to the vehicle in each strain was shown. In Figure 1E–G, the response ratio was estimated by dividing the immobility time of FST-1 by that of FST-2, and responder and nonresponder subgroups were identified via the mean + 2SD method with a cutoff value that was calculated from the data of the vehicle group in each strain.

SPT. Animals were tested for the preference for sucrose using the two-bottle choice paradigm. After a 16-h liquid deprivation, mice were given two bottles, one with 1.5% sucrose and one with tap water. Mice were free to drink liquid from either bottle for 4 h. The right-left position of the two bottles was switched every 2 h. After each test, the bottles were weighed to measure consumption. The preference for sucrose was calculated as the percentage of sucrose solution consumed relative to the total intake.

OFT. Animals were evaluated for locomotion and explorative behavior in an OFT, as reported previously. Mice were individually placed in the center of an open field box (42 cm width × 42 cm depth × 42 cm height) and were allowed to explore the arena freely for 5 min. All animal activity was recorded continuously using a camera placed over the box. Locomotion and the percentage off time

spent in the center were measured automatically using a video-tracking system (ANY-maze, Stoelting).

SIT. Mice were placed in a test chamber (42 cm width × 42 cm depth × 42 cm height) with an empty wire-mesh cage (10 cm width × 6.5 cm depth × 42 cm height) as a first term and were explored for 3 min in the chamber (empty session). After 3 min, test mice were removed and a novel CD1 mouse enclosed in the wire-mesh cage was introduced into the chamber, and the procedure was repeated as a second term (target session). The time spent in the area surrounding the wire-mesh cage (interaction zone, 24 × 14 cm) was measured in both sessions automatically using an ANY-maze tracking system (Stoeling). The SI ratio was calculated by dividing the time spent in the interaction zone of the target session by that of the empty session.

Tissue dissection

Mice treated with IMI, MPR, SRT, DLX or vehicle were euthanized at day 21 (for chronic treatment) or day 5 (for subchronic treatment) of drug treatment. Mice injected with ketamine were euthanized 48h after the ketamine injection (24h after the behavioral test). Mice were anesthetized with isoflurane and whole brains were quickly sliced into 1-mm coronal sections (bregma 1.98–0.98 mm) using a brain matrix (Bio Research Center Co., Ltd.), then further dissected to isolate the medial PFC (mPFC) regions, including the prelimbic, infralimbic, and anterior cingulate (anterior part of Cg1/Cg2) cortices, under a stereomicroscope. mPFC tissue was harvested using a 2-mm-diameter tissue punch (Stoelting) on freshly cut 1-mm-thick coronal sections. Tissues were then snap frozen in liquid nitrogen and were stored at −80°C.

RNA extraction

Total RNA from dissected tissues was extracted using the Direct-zol RNA Microprep (Zymo research), according to the manufacturer's instructions. The quality and concentration of RNA were measured using a NanoDrop (Thermo Fisher Scientific) and the A_{260}/A_{280} ratio was 1.86–2.01 for all RNA preparations.

RNA sequencing (RNA-seq)

Total RNA integrity was determined using an Agilent 2100 Bioanalyzer (Agilent Technology), and the total RNA obtained from each sample was subjected to a sequencing library construction using SureSelect Strand-Specific RNA Library Prep for Illumina (Agilent Technologies, Santa Clara, CA), according to the manufacturer's protocols. The quality of the libraries was assessed using an Agilent 2200 TapeStation High Sensitivity D1000 instrument (Agilent

Technologies, Santa Clara, CA). The pooled libraries of the samples were sequenced using the Illumina HiSeq system in 51-base-pair (bp) single-end reads. Then, sequencing adaptors, low-quality reads, and bases were trimmed with the Trimmomatic-0.32 tool (5). The sequence reads were aligned to the reference mouse genome (mm10) using Tophat 2.0.13 (bowtie2-2.2.3) (6). Files required for the whole-transcriptome alignment with Tophat were downloaded from the Illumina's iGenomes web site (http://support.illumina.com/sequencing/sequencing_software/igenome.html).
For quantifying the gene expression levels and detect differentially expressed genes, the aligned reads were subjected to downstream analyses using the StrandNGS 2.6 software (Agilent Technologies, Santa Clara, CA). The read counts allocated to each gene and transcript (UCSC version 2013.3.6) were quantified using the Trimmed Mean of M-value method (7) implemented in the EdgeR package. DEG analyses were performed using the Limma–Voom method (8, 9). DEG sets were selected when genes were 1.3-fold up/downregulated and the *P*-value was < 0.05 (Figs 2R, 3A–F, S1, and S2) (10-13) or had a Benjamini–Hochberg adjusted *P*-value (FDR *P*) < 0.1 (Fig. 2A, B, J–Q) for comparisons between two groups. A GO profile analysis was applied to DEGs at the biological process level between the vehicle control and SRT-responders (SRT-R), SRT-nonresponders (SRT-NR), DLX-responders (DLX-R), and DLX-nonresponders (DLX-NR) using the goProfiles package (14). To determine the overrepresentation of biological process GO terms, the clusterProfiler package (15) was used with the org.Mm.eg.db annotation package (16). GO terms with a FDR *P* <0.1 were considered to be significantly enriched. The significantly GO enriched terms and DEGs were visualized as network graphs using Gephi (https://gephi.org/) with the Force Atlas layout algorithm. All DEG and GO analyses were performed using the R software, v4.0.5 (http://www.r-project.org/). Raw data were deposited in GEO (GSE168172).

Quantitative PCR (Q-PCR)

cDNA was synthesized from 500 ng of total RNA using the QuantiTect Reverse Transcription Kit (Qiagen), according to the manufacturer's instructions. We performed Q-PCR using the SYBR Green PCR Master Mix (Thermo Fisher Scientific) and a StepOnePlus q-PCR device (Thermo Fisher Scientific). The primer sequences used here are listed in Supplementary Table S1.*β-actin* was used as an internal control.

GFP immunoprecipitation for Ribo-tag

Immunoaffinity purification of ribosomal RNA from the mPFC was carried out as described previously (17), with minor modifications. Protein G dynabeads (Thermo Fischer Scientific) were washed once on a magnetic rack with PBST and then incubated with 2 µl of an anti-GFP antibody (Abcam, ab290) in a total volume of 200 µl of PBST for at least 30 min at room temperature. After the incubation, PBST was removed and the tissue lysates were added to the anti-GFP-conjugated protein G dynabeads, as described below. Mice were anesthetized with isoflurane and mPFC tissues were dissected quickly as described above. mPFCs from 4–6 brains were pooled into one tube, transferred to a Dounce homogenizer, and manually homogenized in 1 ml of ice-cold IP buffer [50 mM Tris, pH 7.5; 1% NP-40; 100 mM KCl; 12 mM $MgCl_2$; 0.5 mM DTT;100 µg/ml cycloheximide (Sigma); 1 mg/ml sodium heparin (Sigma);1x HALT protease inhibitor EDTA-free (Thermo Fischer Scientific); 0.2 U/µl RNasin (Promega)]. Homogenates were transferred to microcentrifuge tubes and clarified at 12,000 x *g* for 10 min at 4°C. Subsequently, 50 µl of the supernatant was taken as the “input”, and the remaining supernatant (approximately 1.5 ml) was used for immunoprecipitation. IP samples were incubated with the anti-GFP conjugated dynabeads for immunoprecipitation (IP fraction) for 2 h at 4°C. Beads were washed three times with Wash Buffer containing 50 mM Tris, pH 7.5; 12 mM $MgCl_2$; 300 mM KCl; 1% NP-40; 0.5 mM DTT; and 100 µg/ml cycloheximide. After the last wash, 500 µl of TRIzol (Thermo Fischer Scientific) was immediately added to the IP fraction and input samples. Total RNA was purified using the Direct-zol RNA Microprep (Zymo research), according to the manufacturers’ instructions.

Viral vector construction

To generate the pAAV-EF1a-DIO-Cartpt-2A-nls-tdTomato plasmid, a DNA fragment encoding GCaMP6f was removed from the pAAV-EF1a-DIO-GCaMP6f-2A-nls-tdTomato plasmid (a gift from Jonathan Ting; Addgene plasmid #51083) and then the Cartpt DNA fragment was inserted. To generate the control pAAV-EF1a-DIO-nls-tdTomato plasmid, a DNA fragment including GCaMP6f and the 2A peptide sequence was removed from the pAAV-EF1a-DIO-GCaMP6f-2A-nls-tdTomato plasmid. To generate the pAAV-Syn-Tet3G-2A-nls-mCherry plasmid, a DNA fragment encoding miniSOG was removed from the pAAV-SYP1-miniSOG-T2A-nls-mCherry plasmid (modified from the pAAV-SYP1-miniSOG-T2A-mCherry plasmid, a gift from Roger Tsien; Addgene plasmid #50972) and then

the Tet3G DNA fragment was inserted (pRetroX-Tet3G Vector plasmid, Clontech). To generate the pAAV-TRE-FLEX-Cartpt-2A-EGFP plasmid, a DNA fragment encoding the Cartpt and 2A peptides (from the pAAV-EF1a-DIO-Cartpt-2A-nls-tdTomato plasmid) was inserted into the pAAV-pTRE-FLEX-EGFP-WPRE plasmid (a gift from Hongkui Zeng; Addgene plasmid #65449). The pAAV-CMV-flag-tTS plasmid was generated by insertion of a DNA fragment encoding tTS (pTet-tTS plasmid, Clontech) into the pAAV-CMV-MCS plasmid (Agilent). The pAAV-Gad1-mCherry plasmid was generated by replacing the DNA fragment of the *Camk2a* promoter in the pAAV-Camk2a-mCherry plasmid (2) with a 1.3 kbp of DNA fragment of the mouse *Gad1* promoter (GenBank accession no. Z49978.1). To generate the pAAV-Gad1-Cartpt-2A-mCherry plasmid, the DNA fragment of the *Camk2a* promoter in the pAAV-Camk2a-TARPγ8-2A-mCherry plasmid (2) was replaced with the DNA fragment of the mouse *Gad1* promoter (from the pAAV-Gad1-mCherry plasmid). Then, the DNA fragment of TARPγ8 in the resulting plasmid (pAAV-Gad1-TARPγ8-2A-mCherry) was further replaced with the *Cartpt* fragment. The genomic titer of each virus was determined using Q-PCR: AAV5-EF1a-DIO-Cartpt-2A-nls-tdTomato (1.1×10^{13} vector genomes (vg)/ml), AAV5-EF1a-DIO-nls-tdTomato (1.5×10^{13} vg/ml), AAV8-Syn-Tet3G-2A-nls-mCherry (2.8×10^{13} vg/ml), AAV5-TRE-FLEX-Cartpt-2A-EGFP (4.1×10^{13} vg/ml), pAAV-CMV-flag-tTS (6.6×10^{13} vg/ml), pAAV-Gad1-mCherry (3.2×10^{13} vg/ml), and pAAV-Gad1-Cartpt-2A-mCherry (6.2×10^{13} vg/ml).

Stereotaxic surgery

Mice were anesthetized with isoflurane (Pfizer; induction, 2%; maintenance, 1.5%) and fixed in a stereotaxic frame (Kopf Instruments). Glass needles were filled with virus solutions. Mice were injected with 0.5 µl of AAVs to the aCC bilaterally at 0.1 µl/min. The needle was left in the injection site for 5 min, for complete diffusion, and was withdrawn slowly. The injection coordinates were: 1.42 mm from Bregma, 0.35 mm lateral from the midline, and 2.3 mm vertical from the cortical surface. The mice were allowed to incubate for at least 3 weeks before experiments.

Histology

Mice were deeply anesthetized with Avertin and transcardially perfused with ice-cold PBS (pH 7.4), followed by a 4% paraformaldehyde (PFA) solution (4°C). Brains were post-fixed in 4% PFA at 4°C for overnight and cryoprotected in 30% PBS-buffered sucrose solution for 48-72 h. The brains were cut into 20-µm thick coronal slices on a cryostat (Leica). Free-floating sections were rinsed in 1x PBS

and mounted on slides and coverslipped with Vectashield (Vector Labs). Images were acquired using a fluorescence microscope (Keyence BZ-X800) and processed with BZ-X800 analyzer software (Keyence), ImageJ, and Adobe Photoshop CS.

RNAscope

Mice were euthanized and brains were dissected, immediately flash-frozen in isopentane chilled with dry ice, and stored at −80°C. Coronal brain slices (20 μm, targeted areas were ranging at bregma 1.70–1.18 mm) were sectioned on a cryostat (Leica) at −20°C, mounted directly onto slides, and stored at −80°C until RNAscope processing. FISH of *Cartpt* and *vGat (Slc32a1)* mRNAs was performed using the RNAscope Fluorescent Multiplex 2.0 assay (Advanced Cell Diagnostics), according to the manufacturer's instructions. Briefly, slides were fixed in 4% PFA and were incubated with protease IV solution and then incubated with appropriate probes for 2 h at 40°C. All probes used in this study were commercially available from Advanced Cell Diagnostics: *Cartpt* (cat#432001-C1), *Camk2a* (cat#411851-C2), and *Slc32a1* (cat#319191-C3). After washing, the signal was amplified by incubating the sections in amplification buffers at 40°C. Slides were coverslipped and images were acquired under a fluorescence microscope (Keyence).

Supplementary References

1. Golden SA, Covington HE, 3rd, Berton O, Russo SJ (2011): A standardized protocol for repeated social defeat stress in mice. *Nat Protoc*. 6:1183-1191.

2. Sakai Y, Li H, Inaba H, Funayama Y, Ishimori E, Kawatake-Kuno A, et al. (2021): Gene-environment interactions mediate stress susceptibility and resilience through the CaMKIIbeta/TARPgamma-8/AMPAR pathway. *iScience*. 24:102504.

3. Uchida S, Hara K, Kobayashi A, Otsuki K, Yamagata H, Hobara T, et al. (2011): Epigenetic status of Gdnf in the ventral striatum determines susceptibility and adaptation to daily stressful events. *Neuron*. 69:359-372.

4. Uchida S, Hara K, Kobayashi A, Fujimoto M, Otsuki K, Yamagata H, et al. (2011): Impaired hippocampal spinogenesis and neurogenesis and altered affective behavior in mice lacking heat shock factor 1. *Proc Natl Acad Sci U S A*. 108:1681-1686.

5. Bolger AM, Lohse M, Usadel B (2014): Trimmomatic: a flexible trimmer

for Illumina sequence data. *Bioinformatics*. 30:2114-2120.
6. Langmead B, Salzberg SL (2012): Fast gapped-read alignment with Bowtie 2. *Nat Methods*. 9:357-359.
7. Robinson MD, Oshlack A (2010): A scaling normalization method for differential expression analysis of RNA-seq data. *Genome Biol*. 11:R25.
8. Law CW, Chen Y, Shi W, Smyth GK (2014): voom: Precision weights unlock linear model analysis tools for RNA-seq read counts. *Genome Biol*. 15:R29.
9. Ritchie ME, Phipson B, Wu D, Hu Y, Law CW, Shi W, et al. (2015): limma powers differential expression analyses for RNA-sequencing and microarray studies. *Nucleic Acids Res*. 43:e47.
10. Bagot RC, Cates HM, Purushothaman I, Vialou V, Heller EA, Yieh L, et al. (2017): Ketamine and Imipramine Reverse Transcriptional Signatures of Susceptibility and Induce Resilience-Specific Gene Expression Profiles. *Biol Psychiatry*. 81:285-295.
11. van der Zee YY, Lardner CK, Parise EM, Mews P, Ramakrishnan A, Patel V, et al. (2021): Sex-Specific Role for SLIT1 in Regulating Stress Susceptibility. *Biol Psychiatry*.
12. Issler O, van der Zee YY, Ramakrishnan A, Wang J, Tan C, Loh YE, et al. (2020): Sex-Specific Role for the Long Non-coding RNA LINC00473 in Depression. *Neuron*. 106:912-926 e915.
13. Walker DM, Cunningham AM, Nestler EJ (2021): Reply to: Multiple Comparisons and Inappropriate Statistical Testing Lead to Spurious Sex Differences in Gene Expression. *Biol Psychiatry*.
14. Alex Sanchez JOaMS (2020): goProfiles: goProfiles: an R package for the statistical analysis of functional profiles. *R package version*. 1.52.0.
15. Yu G, Wang LG, Han Y, He QY (2012): clusterProfiler: an R package for comparing biological themes among gene clusters. *OMICS*. 16:284-287.
16. Carlson M (2020): org.Mm.eg.db: Genome wide annotation for Mouse. *R package version* 3.12.0.
17. Ye L, Allen WE, Thompson KR, Tian Q, Hsueh B, Ramakrishnan C, et al. (2016): Wiring and Molecular Features of Prefrontal Ensembles Representing Distinct Experiences. *Cell*. 165:1776-1788.

Supplementary Figures

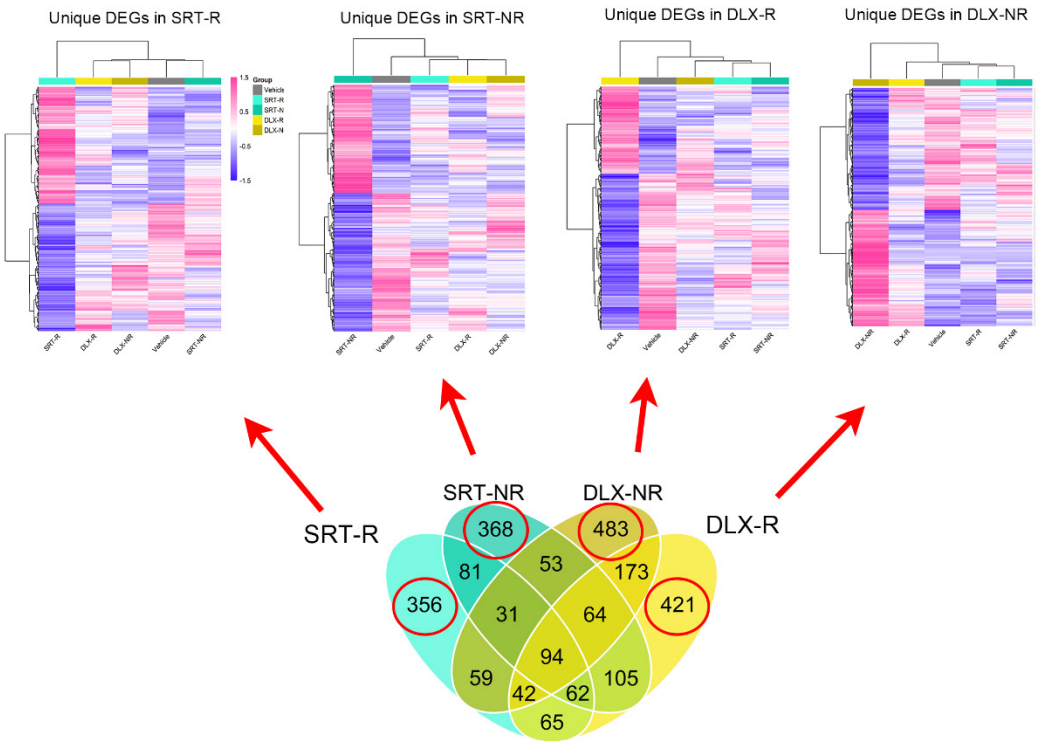

Figure S1. Heatmap of RNA-seq data.
Heatmap showing differentially regulated genes (fold change >1.3 and $p < 0.05$) that were specifically regulated in SRT or DLX treatment responders or nonresponders.

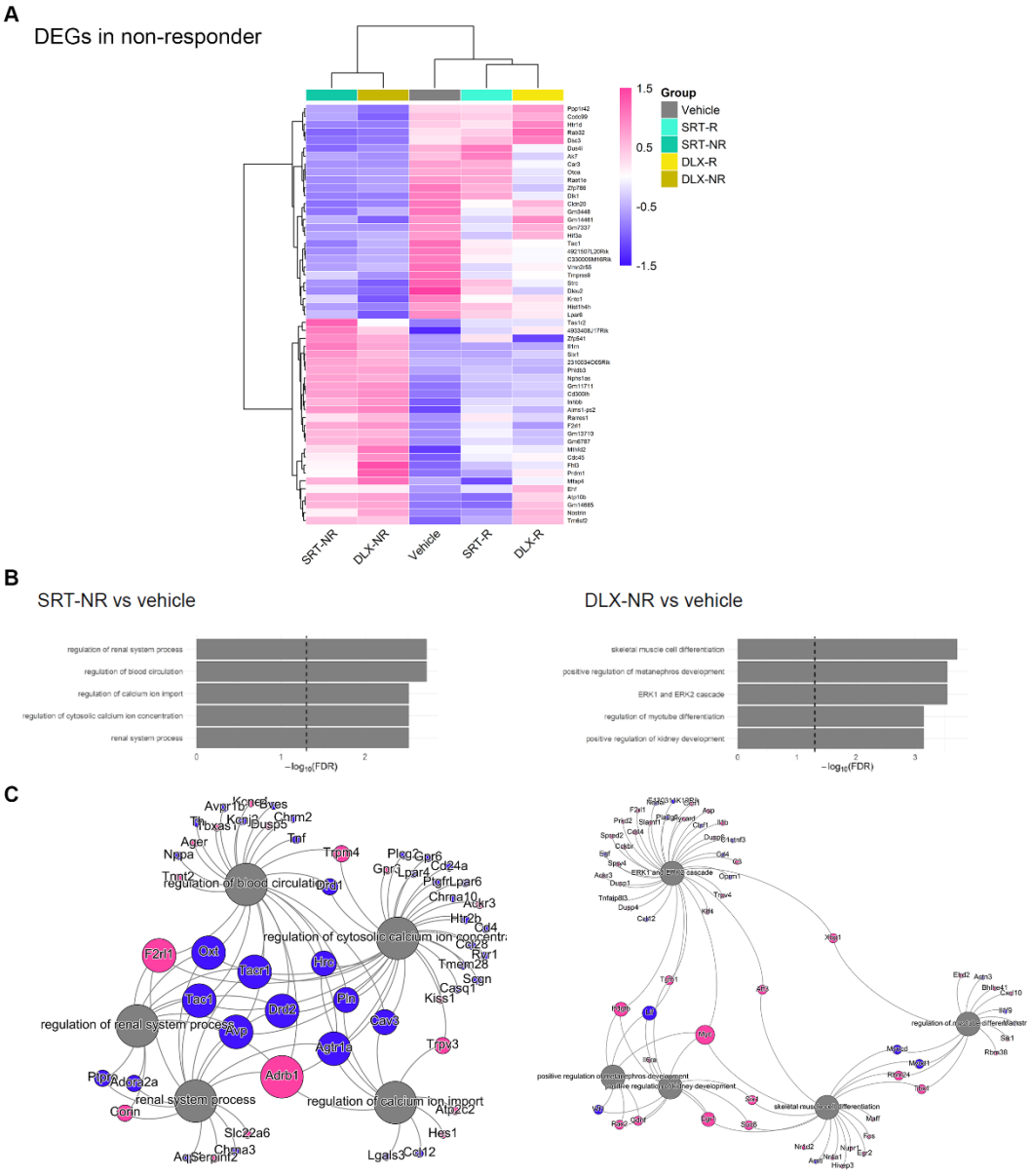

Figure S2. Differentially expressed genes in antidepressant treatment nonresponders.

A. Heatmap showing the differentially expressed genes (fold change >1.3 and $p < 0.05$) that were consistently regulated in SRT and DLX treatment nonresponders, but not in SRT or DLX treatment responders.

B and C. GO enrichment analysis (B) and network graph visualization (C) of differentially expressed genes that were regulated in SRT or DLX treatment nonresponders. Top-five significant GO terms associated with differentially expressed genes in SRT-NR and DLX-NR.

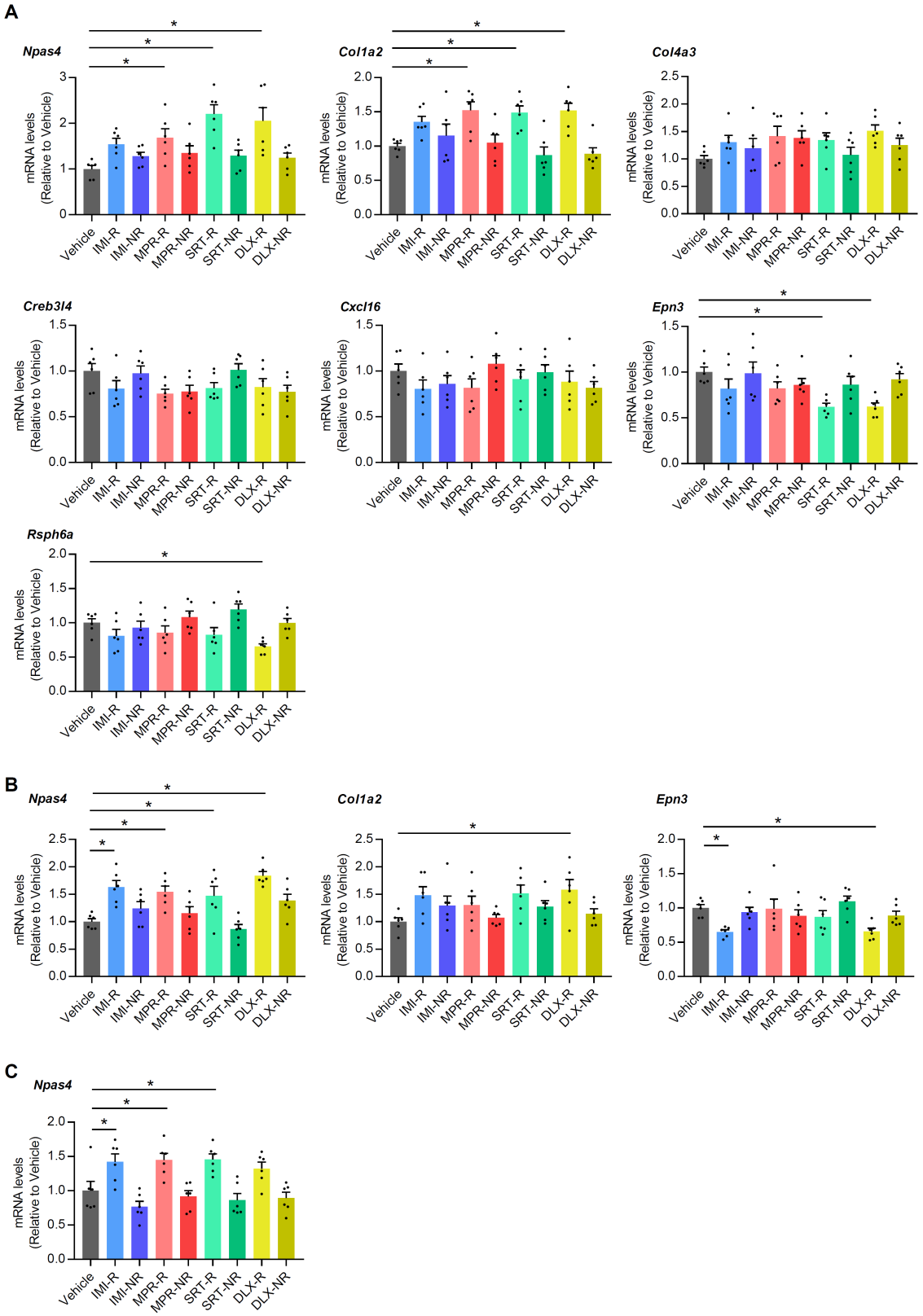

Figure S3. Q-PCR validation of RNA-seq data.

A. Q-PCR analysis of *Npas4, Col1a2*, *Col4a3*, *Creb3l4*, *Cxcl16*, and *Epn3,* and

Rsph6a in the mPFC of IMI-, MPR-, SRT-, and DLX-responders and nonresponders in BALB mice. n = 4–6 in each group. *Adjusted $p < 0.05$ vs. the vehicle.

B. Q-PCR analysis of *Npas4, Col1a2*, and *Epn3* mRNA expression in the mPFC of IMI-, MPR-, SRT-, and DLX-responders and nonresponders in B6 mice. n = 6 in each group. *$p < 0.05$ vs. the vehicle.

C. Q-PCR analysis of *Npas4* mRNA expression in the mPFC of IMI-, MPR-, SRT-, and DLX-responders and nonresponders in DBA mice. n = 6 in each group. *$p < 0.05$ vs. the vehicle.

The bar graphs show the mean ± SEM.

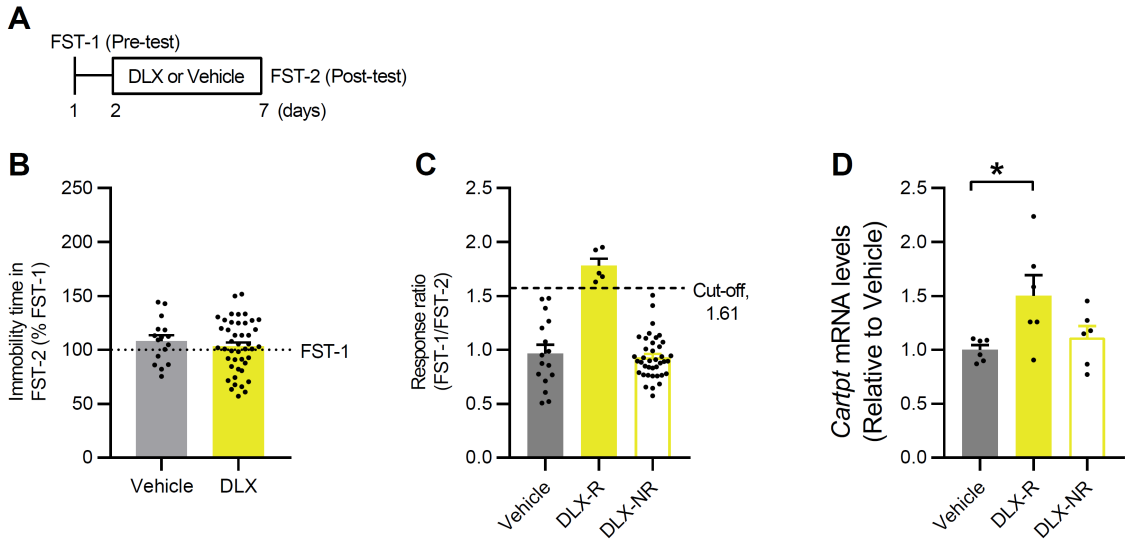

Figure S4. Effects of subchronic treatment with duloxetine on immobility duration in the FST and *Cartpt* expression in B6 mice

A. Experimental design. B6 mice were tested by forced swim test (FST-1) prior to a 5-day treatment with either tap water (V) or duloxetine (DLX). After the treatment with antidepressants, a second forced swim test (FST-2) was performed.

B. Immobility time in the FST-2 (% FST-1) in B6 mice is shown. n = 16–44 in each group. **p* < 0.05 vs. FST-1 in the corresponding treatment.

C. Response ratio (immobility time in FST-1 / immobility time in FST-2) is shown. The responder and nonresponder subgroups were identified by the mean + 2SD method with a cutoff value. n = 60 in total.

D. Q-PCR revealed the upregulation of *Cartpt* in the mPFC of DLX-responders, but not in nonresponders. n = 5–6 in each group. **p* < 0.05 vs. the vehicle.

Bar graphs show the mean ± SEM.

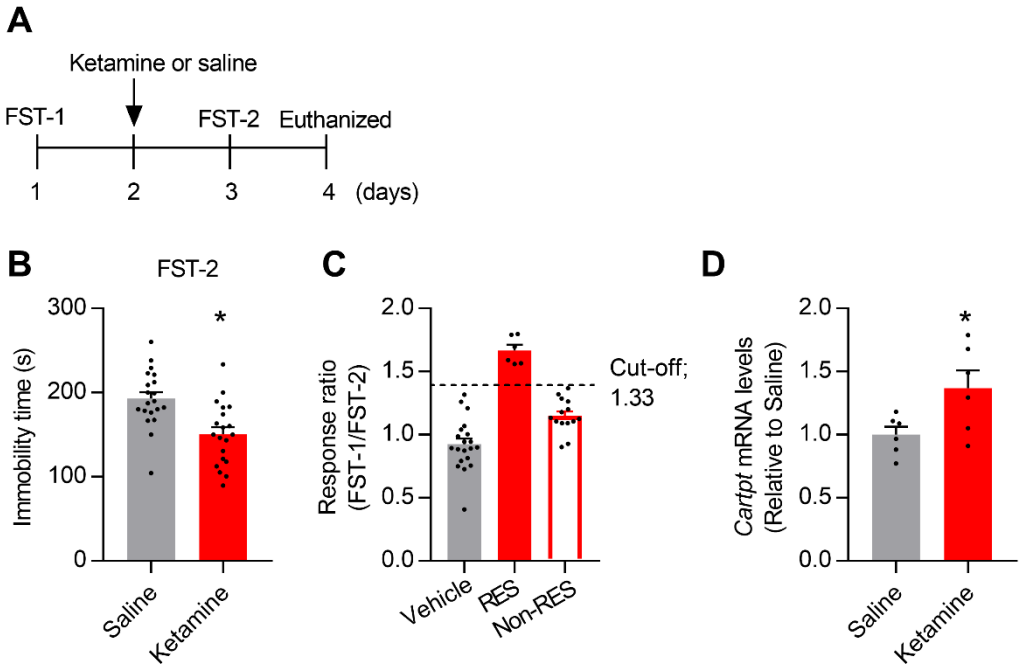

Figure S5. Ketamine increased *Cartpt* expression in the mPFC.

A. Experimental design. BALB mice were tested by forced swim test (FST-1) prior to a single treatment with ketamine or saline. After the treatment with ketamine, a second forced swim test (FST-2) was performed.

B. Immobility time in the forced swim test was reduced at 24 h after ketamine treatment in BALB mice. n = 20 in each group. **p* < 0.05.

C. The response ratio (immobility time in FST-1 / immobility time in FST-2) is shown. The responder and nonresponder subgroups were identified by the mean + 2SD method with a cutoff value.

D. Q-PCR quantification of *Cartpt* expression in the mPFC of ketamine responders. n = 6 samples in each group. **p* < 0.05.

Bar graphs show the mean ± SEM.

Legends of Supplementary Tables (see Excel files)

Table S1. List of primer sequences used for Q-PCR.

Table S2. Complete statistical analysis.

Table S3. Differentially expressed genes that were (a) commonly regulated in sertraline (SRT) and duloxetine (DLX) treatment responders and nonresponders and (b) regulated in SRT or DLX treatment responders or nonresponders.

Table S4. Differentially expressed genes that are uniquely regulated in sertraline (SRT) or duloxetine (DLX) treatment responders or nonresponders.

Table S5. Differentially expressed genes that are (a) commonly regulated in sertraline (SRT) and duloxetine (DLX) treatment responders, as represented in Figure 3B, and (b) commonly regulated in SRT and DLX treatment nonresponders.

Table S6. Differentially expressed genes that are regulated in sertraline (SRT) or duloxetine (DLX) treatment responders but not in the corresponding nonresponders.

Table S7. Differentially expressed genes that are regulated in sertraline (SRT) or duloxetine (DLX) treatment nonresponders but not in the corresponding responders.